

PRE-TRAINING MOLECULAR GRAPH REPRESENTATION WITH 3D GEOMETRY

Shengchao Liu^{1,2}, Hanchen Wang³, Weiyang Liu^{3,4}, Joan Lasenby³, Hongyu Guo⁵, Jian Tang^{1,6,7}

¹Mila ²Université de Montréal ³University of Cambridge ⁴MPI for Intelligent Systems, Tübingen

⁵National Research Council Canada ⁶HEC Montréal ⁷CIFAR AI Chair

ABSTRACT

Molecular graph representation learning is a fundamental problem in modern drug and material discovery. Molecular graphs are typically modeled by their 2D topological structures, but it has been recently discovered that 3D geometric information plays a more vital role in predicting molecular functionalities. However, the lack of 3D information in real-world scenarios has significantly impeded the learning of geometric graph representation. To cope with this challenge, we propose the Graph Multi-View Pre-training (GraphMVP) framework where self-supervised learning (SSL) is performed by leveraging the correspondence and consistency between 2D topological structures and 3D geometric views. GraphMVP effectively learns a 2D molecular graph encoder that is enhanced by richer and more discriminative 3D geometry. We further provide theoretical insights to justify the effectiveness of GraphMVP. Finally, comprehensive experiments show that GraphMVP can consistently outperform existing graph SSL methods. Code is available on [GitHub](#).

1 INTRODUCTION

In recent years, drug discovery has drawn increasing interest in the machine learning community. Among many challenges therein, how to discriminatively represent a molecule with a vectorized embedding remains a fundamental yet open challenge. The underlying problem can be decomposed into two components: how to design a common latent space for molecule graphs (*i.e.*, designing a suitable encoder) and how to construct an objective function to supervise the training (*i.e.*, defining a learning target). Falling broadly into the second category, our paper studies self-supervised molecular representation learning by leveraging the consistency between 3D geometry and 2D topology.

Motivated by the prominent success of the pretraining-finetuning pipeline [17], unsupervisedly pre-trained graph neural networks for molecules yields promising performance on downstream tasks and becomes increasingly popular [42, 54, 82, 90, 103, 104]. The key to pre-training lies in finding an effective proxy task (*i.e.*, training objective) to leverage the power of large unlabeled datasets. Inspired by [54, 58, 79] that molecular properties [29, 54] can be better predicted by 3D geometry due to its encoded energy knowledge, we aim to make use of the 3D geometry of molecules in pre-training. However, the stereochemical structures are often very expensive to obtain, making such 3D geometric information scarce in downstream tasks. To address this problem, we propose the Graph Multi-View Pre-training (GraphMVP) framework, where a 2D molecule encoder is pre-trained with the knowledge of 3D geometry and then fine-tuned on downstream tasks without 3D information. Our learning paradigm, during pre-training, injects the knowledge of 3D molecular geometry to a 2D molecular graph encoder such that the downstream tasks can benefit from the implicit 3D geometric prior even if there is no 3D information available.

We attain the aforementioned goal by leveraging two pretext tasks on the 2D and 3D molecular graphs: one contrastive and one generative SSL. Contrastive SSL creates the supervised signal at an **inter-molecule** level: the 2D and 3D graph pairs are positive if they are from the same molecule, and negative otherwise; Then contrastive SSL [93] will align the positive pairs and contrast the negative pairs simultaneously. Generative SSL [38, 49, 91], on the other hand, obtains the supervised signal in an **intra-molecule** way: it learns a 2D/3D representation that can reconstruct its 3D/2D counterpart view for each molecule itself. To cope with the challenge of measuring the quality of reconstruction on molecule 2D and 3D space, we further propose a novel surrogate objective function called variation

representation reconstruction (VRR) for the generative SSL task, which can effectively measure such quality in the continuous representation space. The knowledge acquired by these two SSL tasks is complementary, so our GraphMVP framework integrates them to form a more discriminative 2D molecular graph representation. Consistent and significant performance improvements empirically validate the effectiveness of GraphMVP.

We give additional insights to justify the effectiveness of GraphMVP. First, GraphMVP is a self-supervised learning approach based on maximizing mutual information (MI) between 2D and 3D views, enabling the learnt representation to capture high-level factors [6, 7, 86] in molecule data. Second, we find that 3D molecular geometry is a form of privileged information [88, 89]. It has been proven that using privileged information in training can accelerate the speed of learning. We note that privileged information is only used in training, while it is not available in testing. This perfectly matches our intuition of pre-training molecular representation with 3D geometry.

Our contributions include (1) To our best knowledge, we are the first to incorporate the 3D geometric information into graph SSL; (2) We propose one contrastive and one generative SSL tasks for pre-training. Then we elaborate their difference and empirically validate that combining both can lead to a better representation; (3) We provide theoretical insights and case studies to justify why adding 3D geometry is beneficial; (4) We achieve the SOTA performance among all the SSL methods.

Related work. We briefly review the most related works here and include a more detailed summarization in Appendix A. Self-supervised learning (SSL) methods have attracted massive attention to graph applications [57, 59, 97, 99]. In general, there are roughly two categories of graph SSL: contrastive and generative, where they differ on the design of the supervised signals. Contrastive graph SSL [42, 82, 90, 103, 104] constructs the supervised signals at the **inter-graph** level and learns the representation by contrasting with other graphs, while generative graph SSL [34, 42, 43, 54] focuses on reconstructing the original graph at the **intra-graph** level. One of the most significant differences that separate our work from existing methods is that all previous methods **merely** focus on 2D molecular topology. However, for scientific tasks such as molecular property prediction, 3D geometry should be incorporated as it provides complementary and comprehensive information [58, 79]. To fill this gap, we propose GraphMVP to leverage the 3D geometry in graph self-supervised pre-training.

2 PRELIMINARIES

We first outline the key concepts and notations used in this work. Self-supervised learning (SSL) is based on the *view* design, where each view provides a specific aspect and modality of the data. Each molecule has two natural views: the 2D graph incorporates the topological structure defined by the adjacency, while the 3D graph can better reflect the geometry and spatial relation. From a chemical perspective, 3D geometric graphs focus on the *energy* while 2D graphs emphasize the *topological* information; thus they can be composed for learning more informative representation in GraphMVP. *Transformation* is an atomic operation in SSL that can extract specific information from each view. Next, we will briefly introduce how to represent these two views.

2D Molecular Graph represents molecules as 2D graphs, with atoms as nodes and bonds as edges respectively. We denote each 2D graph as $g_{2D} = (X, E)$, where X is the atom attribute matrix and E is the bond attribute matrix. Notice that here E also includes the bond connectivity. Then we will apply a transformation function T_{2D} on the topological graph. Given a 2D molecular graph g_{2D} , its representation h_{2D} can be obtained from a *2D graph neural network (GNN)* model:

$$h_{2D} = \text{GNN-2D}(T_{2D}(g_{2D})) = \text{GNN-2D}(T_{2D}(X, E)). \quad (1)$$

3D Molecular Graph additionally includes spatial positions of the atoms, and they are needless to be static since atoms are in continual motion on *a potential energy surface* [4]. ¹ The 3D structures at the local minima on this surface are named *conformer*. As the molecular properties are conformers ensembled [36], GraphMVP provides a novel perspective on adopting 3D conformers for learning better representation. Given a conformer $g_{3D} = (X, R)$, its representation via a *3D GNN* model is:

$$h_{3D} = \text{GNN-3D}(T_{3D}(g_{3D})) = \text{GNN-3D}(T_{3D}(X, R)), \quad (2)$$

¹A more rigorous way of defining conformer is in [65]: a conformer is an isomer of a molecule that differs from another isomer by the rotation of a single bond in the molecule.

where R is the 3D-coordinate matrix and T_{3D} is the 3D transformation. In what follows, for notation simplicity, we use x and y for the 2D and 3D graphs, *i.e.*, $x \triangleq g_{2D}$ and $y \triangleq g_{3D}$. Then the latent representations are denoted as h_x and h_y .

3 GRAPHMVP: GRAPH MULTI-VIEW PRE-TRAINING

Our model, termed as Graph Multi-View Pre-training (GraphMVP), conducts self-supervised learning (SSL) pre-training with 3D information. The 3D conformers encode rich information about the molecule energy and spatial structure, which are complementary to the 2D topology. Thus, applying SSL between the 2D and 3D views will provide a better 2D representation, which implicitly embeds the ensembles of energies and geometric information for molecules.

In the following, we first present an overview of GraphMVP, and then introduce two pretext tasks specialized concerning 3D conformation structures. Finally, we summarize a broader graph SSL family that prevails the 2D molecular graph representation learning with 3D geometry.

3.1 OVERVIEW OF GRAPHMVP

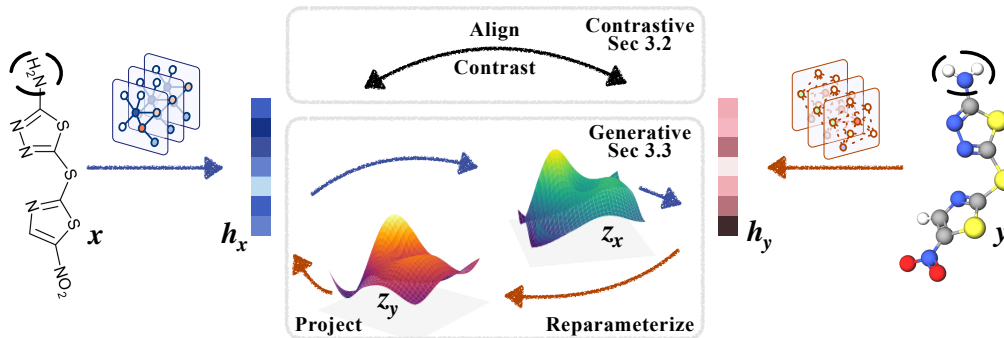


Figure 1: Overview of the pre-training stage in GraphMVP. The black dashed circles denote subgraph masking, and we mask the same region in the 2D and 3D graphs. Multiple views of the molecules (herein: Halicin) are mapped to the representation space via 2D and 3D GNN models, where we conduct GraphMVP for SSL pre-training, using both contrastive and generative pretext tasks.

In general, GraphMVP exerts 2D topology and 3D geometry as two complementary views for each molecule. By performing SSL between these views, it is expected to learn a 2D representation enhanced with 3D conformation, which can better reflect certain molecular properties.

As generic SSL pre-training pipelines, GraphMVP has two stages: pre-training then fine-tuning. In the pre-training stage, we conduct SSL via auxiliary tasks on data collections that provide both 2D and 3D molecular structures. During fine-tuning, the pre-trained 2D GNN models are subsequently fine-tuned on specific downstream tasks, where only 2D molecular graphs are available.

At the SSL pre-training stage, we design two pretext tasks: one contrastive and one generative. We conjecture and then empirically prove that these two tasks are focusing on different learning aspects, which are summarized into the following two points. (1) From the perspective of representation learning, contrastive SSL utilizes **inter-data** knowledge and generative SSL utilizes **intra-data** knowledge. For contrastive SSL, one key step is to obtain the negative view pairs for inter-data contrasting; while generative SSL focuses on each data point itself, by reconstructing the key features at an intra-data level. (2) From the perspective of distribution learning, contrastive SSL and generative SSL are learning the data distribution from a **local** and **global** manner, respectively. Contrastive SSL learns the distribution locally by contrasting the pairwise distance at an inter-data level. Thus, with sufficient number of data points, the local contrastive operation can iteratively recover the data distribution. Generative SSL, on the other hand, learns the global data density function directly.

Therefore, contrastive and generative SSL are essentially conducting representation and distribution learning with different intuitions and disciplines, and we expect that combining both can lead to a better representation. We later carry out an ablation study (Section 4.4) to verify this empirically. In

addition, to make the pretext tasks more challenging, we take views for each molecule by randomly masking M nodes (and corresponding edges) as the transformation function, *i.e.*, $T_{2D} = T_{3D} = \text{mask}$. This trick has been widely used in graph SSL [42, 103, 104] and has shown robust improvements.

3.2 CONTRASTIVE SELF-SUPERVISED LEARNING BETWEEN 2D AND 3D VIEWS

The main idea of contrastive self-supervised learning (SSL) [10, 69] is first to define positive and negative pairs of views from an inter-data level, and then to align the positive pairs and contrast the negative pairs simultaneously [93]. For each molecule, we first extract representations from 2D and 3D views, *i.e.*, h_x and h_y . Then we create positive and negative pairs for contrastive learning: the 2D-3D pairs (x, y) for the same molecule are treated as positive, and negative otherwise. Finally, we align the positive pairs and contrast the negative ones. The pipeline is shown in Figure 1. In the following, we discuss two common objective functions on contrastive graph SSL.

InfoNCE is first proposed in [69], and its effectiveness has been validated both empirically [10, 37] and theoretically [3]. Its formulation is given as follows:

$$\mathcal{L}_{\text{InfoNCE}} = -\frac{1}{2}\mathbb{E}_{p(x,y)}\left[\log \frac{\exp(f_x(x,y))}{\exp(f_x(x,y)) + \sum_j \exp(f_x(x^j, y))} + \log \frac{\exp(f_y(y,x))}{\exp(f_y(y,x)) + \sum_j \exp(f_y(y^j, x))}\right], \quad (3)$$

where x^j, y^j are randomly sampled 2D and 3D views regarding to the anchored pair (x, y) . $f_x(x, y)$ and $f_y(y, x)$ are scoring functions for the two corresponding views, with flexible formulations. Here we adopt $f_x(x, y) = f_y(y, x) = \langle h_x, h_y \rangle$. More details are in Appendix D.

Energy-Based Model with Noise Contrastive Estimation (EBM-NCE) is an alternative that has been widely used in the line of graph contrastive SSL [42, 82, 103, 104]. Its intention is essentially the same as InfoNCE, to align positive pairs and contrast negative pairs, while the main difference is the usage of binary cross-entropy and extra noise distribution for negative sampling:

$$\begin{aligned} \mathcal{L}_{\text{EBM-NCE}} = & -\frac{1}{2}\mathbb{E}_{p(y)}\left[\mathbb{E}_{p_n(x|y)} \log(1 - \sigma(f_x(x, y))) + \mathbb{E}_{p(x|y)} \log \sigma(f_x(x, y))\right] \\ & -\frac{1}{2}\mathbb{E}_{p(x)}\left[\mathbb{E}_{p_n(y|x)} \log(1 - \sigma(f_y(y, x))) + \mathbb{E}_{p(y|x)} \log \sigma(f_y(y, x))\right], \end{aligned} \quad (4)$$

where p_n is the noise distribution and σ is the sigmoid function. We also notice that the final formulation of EBM-NCE shares certain similarities with Jensen-Shannon estimation (JSE) [68]. However, the derivation process and underlying intuition are different: EBM-NCE models the conditional distributions in MI lower bound (Equation (9)) with EBM, while JSE is a special case of variational estimation of f-divergence. Since this is not the main focus of GraphMVP, we expand the a more comprehensive comparison in Appendix D, plus the potential benefits with EBM-NCE.

Few works [35] have witnessed the effect on the choice of objectives in graph contrastive SSL. In GraphMVP, we treat it as a hyper-parameter and further run ablation studies on them, *i.e.*, to solely use either InfoNCE ($\mathcal{L}_C = \mathcal{L}_{\text{InfoNCE}}$) or EMB-NCE ($\mathcal{L}_C = \mathcal{L}_{\text{EBM-NCE}}$).

3.3 GENERATIVE SELF-SUPERVISED LEARNING BETWEEN 2D AND 3D VIEWS

Generative SSL is another classic track for unsupervised pre-training [11, 48, 49, 51]. It aims at learning an effective representation by self-reconstructing each data point. Specifically to drug discovery, we have one 2D graph and a certain number of 3D conformers for each molecule, and our goal is to learn a robust 2D/3D representation that can, to the most extent, recover its 3D/2D counterparts. By doing so, generative SSL can enforce 2D/3D GNN to encode the most crucial geometry/topology information, which can improve the downstream performance.

There are many options for generative models, including variational auto-encoder (VAE) [49], generative adversarial networks (GAN) [30], flow-based model [18], etc. In GraphMVP, we prefer VAE-like method for the following reasons: (1) The mapping between two molecular views is stochastic: multiple 3D conformers correspond to the same 2D topology; (2) An explicit 2D graph representation (*i.e.*, feature encoder) is required for downstream tasks; (3) Decoders for structured data such as graph are often highly nontrivial to design, which make them a suboptimal choice.

Variational Molecule Reconstruction. Therefore we propose a *light* VAE-like generative SSL, equipped with a *crafty* surrogate loss, which we describe in the following. We start with an example

for illustration. When generating 3D conformers from their corresponding 2D topology, we want to model the conditional likelihood $p(\mathbf{y}|\mathbf{x})$. By introducing a reparameterized variable $\mathbf{z}_x = \mu_x + \sigma_x \odot \epsilon$, where μ_x and σ_x are two flexible functions on h_x , $\epsilon \sim \mathcal{N}(0, I)$ and \odot is the element-wise production, we have the following lower bound:

$$\log p(\mathbf{y}|\mathbf{x}) \geq \mathbb{E}_{q(\mathbf{z}_x|\mathbf{x})} [\log p(\mathbf{y}|\mathbf{z}_x)] - KL(q(\mathbf{z}_x|\mathbf{x})||p(\mathbf{z}_x)). \quad (5)$$

The expression for $\log p(\mathbf{x}|\mathbf{y})$ can be similarly derived. Equation (5) includes a conditional log-likelihood and a KL-divergence term, where the bottleneck is to calculate the first term for structured data. This term has also been recognized as the *reconstruction term*: it is essentially to reconstruct the 3D conformers (\mathbf{y}) from the sampled 2D molecular graph representation (\mathbf{z}_x). However, performing the graph reconstruction on the data space is not trivial: since molecules (e.g., atoms and bonds) are discrete, modeling and measuring on the molecule space will bring extra obstacles.

Variational Representation Reconstruction (VRR). To cope with this challenge, we propose a novel surrogate loss by switching the reconstruction from data space to representation space. Instead of decoding the latent code \mathbf{z}_x to data space, we can directly project it to the 3D representation space, denoted as $q_x(\mathbf{z}_x)$. Since the representation space is continuous, we may as well model the conditional log-likelihood with Gaussian distribution, resulting in L2 distance for reconstruction, i.e., $\|q_x(\mathbf{z}_x) - SG(h_y(\mathbf{y}))\|^2$. Here SG is the stop-gradient operation, assuming that h_y is a fixed learnt representation function. SG has been widely adopted in the SSL literature to avoid model collapse [12, 31]. We call this surrogate loss as variational representation reconstruction (VRR):

$$\begin{aligned} \mathcal{L}_G = \mathcal{L}_{VRR} &= \frac{1}{2} \left[\mathbb{E}_{q(\mathbf{z}_x|\mathbf{x})} [\|q_x(\mathbf{z}_x) - SG(h_y)\|^2] + \mathbb{E}_{q(\mathbf{z}_y|\mathbf{y})} [\|q_y(\mathbf{z}_y) - SG(h_x)\|_2^2] \right] \\ &\quad + \frac{\beta}{2} \cdot [KL(q(\mathbf{z}_x|\mathbf{x})||p(\mathbf{z}_x)) + KL(q(\mathbf{z}_y|\mathbf{y})||p(\mathbf{z}_y))]. \end{aligned} \quad (6)$$

We give a simplified illustration for the generative SSL pipeline in Figure 1 and the complete derivations in Appendix E. As will be discussed in Section 5.1, VRR is actually maximizing MI, and MI is invariant to continuous bijective function [7]. Thus, this surrogate loss would be exact if the encoding function h satisfies this condition. However, we find that GNN, though does not meet the condition, can provide quite robust performance, which empirically justify the effectiveness of VRR.

3.4 MULTI-TASK OBJECTIVE FUNCTION

As discussed before, contrastive SSL and generative SSL essentially learn the representation from distinct viewpoints. A reasonable conjecture is that combining both SSL methods can lead to overall better performance, thus we arrive at minimizing the following complete objective for GraphMVP:

$$\mathcal{L}_{GraphMVP} = \alpha_1 \cdot \mathcal{L}_C + \alpha_2 \cdot \mathcal{L}_G, \quad (7)$$

where α_1, α_2 are weighting coefficients. A later performed ablation study (Section 4.4) delivers two important messages: (1) Both individual contrastive and generative SSL on 3D conformers can consistently help improve the 2D representation learning; (2) Combining the two SSL strategies can yield further improvements. Thus, we draw the conclusion that GraphMVP (Equation (7)) is able to obtain an augmented 2D representation by fully utilizing the 3D information.

As discussed in Section 1, existing graph SSL methods only focus on the 2D topology, which is in parallel to GraphMVP: 2D graph SSL focuses on exploiting the 2D structure topology, and GraphMVP takes advantage of the 3D geometry information. Thus, we propose to merge the 2D SSL into GraphMVP. Since there are two main categories in 2D graph SSL: generative and contrastive, we propose two variants GraphMVP-G and GraphMVP-C accordingly. Their objectives are as follows:

$$\mathcal{L}_{GraphMVP-G} = \mathcal{L}_{GraphMVP} + \alpha_3 \cdot \mathcal{L}_{Generative\ 2D-SSL}, \quad \mathcal{L}_{GraphMVP-C} = \mathcal{L}_{GraphMVP} + \alpha_3 \cdot \mathcal{L}_{Contrastive\ 2D-SSL}. \quad (8)$$

Later, the empirical results also help support the effectiveness of GraphMVP-G and GraphMVP-C, and thus, we can conclude that existing 2D SSL is complementary to GraphMVP.

4 EXPERIMENTS AND RESULTS

4.1 EXPERIMENTAL SETTINGS

Datasets. We pre-train models on the same dataset then fine-tune on the wide range of downstream tasks. We randomly select 50k qualified molecules from GEOM [4] with both 2D and 3D structures

Table 1: Results for molecular property prediction tasks. For each downstream task, we report the mean (and standard deviation) ROC-AUC of 3 seeds with scaffold splitting. For GraphMVP, we set $M = 0.15$ and $C = 5$. The best and second best results are marked **bold** and **bold**, respectively.

Pre-training	BBBP	Tox21	ToxCast	Sider	ClinTox	MUV	HIV	Bace	Avg
-	65.4(2.4)	74.9(0.8)	61.6(1.2)	58.0(2.4)	58.8(5.5)	71.0(2.5)	75.3(0.5)	72.6(4.9)	67.21
EdgePred	64.5(3.1)	74.5(0.4)	60.8(0.5)	56.7(0.1)	55.8(6.2)	73.3(1.6)	75.1(0.8)	64.6(4.7)	65.64
AttrMask	70.2(0.5)	74.2(0.8)	62.5(0.4)	60.4(0.6)	68.6(9.6)	73.9(1.3)	74.3(1.3)	77.2(1.4)	70.16
GPT-GNN	64.5(1.1)	75.3(0.5)	62.2(0.1)	57.5(4.2)	57.8(3.1)	76.1(2.3)	75.1(0.2)	77.6(0.5)	68.27
InfoGraph	69.2(0.8)	73.0(0.7)	62.0(0.3)	59.2(0.2)	75.1(5.0)	74.0(1.5)	74.5(1.8)	73.9(2.5)	70.10
ContextPred	71.2(0.9)	73.3(0.5)	62.8(0.3)	59.3(1.4)	73.7(4.0)	72.5(2.2)	75.8(1.1)	78.6(1.4)	70.89
GraphLoG	67.8(1.7)	73.0(0.3)	62.2(0.4)	57.4(2.3)	62.0(1.8)	73.1(1.7)	73.4(0.6)	78.8(0.7)	68.47
G-Contextual	70.3(1.6)	75.2(0.3)	62.6(0.3)	58.4(0.6)	59.9(8.2)	72.3(0.9)	75.9(0.9)	79.2(0.3)	69.21
G-Motif	66.4(3.4)	73.2(0.8)	62.6(0.5)	60.6(1.1)	77.8(2.0)	73.3(2.0)	73.8(1.4)	73.4(4.0)	70.14
GraphCL	67.5(3.3)	75.0(0.3)	62.8(0.2)	60.1(1.3)	78.9(4.2)	77.1(1.0)	75.0(0.4)	68.7(7.8)	70.64
JOAO	66.0(0.6)	74.4(0.7)	62.7(0.6)	60.7(1.0)	66.3(3.9)	77.0(2.2)	76.6(0.5)	72.9(2.0)	69.57
GraphMVP	68.5(0.2)	74.5(0.4)	62.7(0.1)	62.3(1.6)	79.0(2.5)	75.0(1.4)	74.8(1.4)	76.8(1.1)	71.69
GraphMVP-G	70.8(0.5)	75.9(0.5)	63.1(0.2)	60.2(1.1)	79.1(2.8)	77.7(0.6)	76.0(0.1)	79.3(1.5)	72.76
GraphMVP-C	72.4(1.6)	74.4(0.2)	63.1(0.4)	63.9(1.2)	77.5(4.2)	75.0(1.0)	77.0(1.2)	81.2(0.9)	73.07

for the pre-training. As clarified in Section 3.1, conformer ensembles can better reflect the molecular property, thus we take C conformers of each molecule. For downstream tasks, we first stick to the same setting of the main graph SSL work [42, 103, 104], exploring 8 binary molecular property prediction tasks, which are all in the low-data regime. Then we explore 6 regression tasks from various low-data domains to be more comprehensive. We describe all the datasets in Appendix F.

2D GNN. We follow the research line of SSL on molecule graph [42, 103, 104], using the same Graph Isomorphism Network (GIN) [100] as the backbone model, with the same feature sets.

3D GNN. We choose SchNet [79] for geometric modeling, since SchNet: (1) is found to be a strong geometric representation learning method under the fair benchmarking; (2) can be trained more efficiently, comparing to the other recent 3D models. More detailed explanations are in Appendix B.2.

4.2 MAIN RESULTS ON MOLECULAR PROPERTY PREDICTION.

We carry out comprehensive comparisons with 10 SSL baselines and random initialization. For pre-training, we apply all SSL methods on the same dataset based on GEOM [4]. For fine-tuning, we follow the same setting [42, 103, 104] with 8 low-data molecular property prediction tasks.

Baselines. Due to the rapid growth of graph SSL [59, 97, 99], we are only able to benchmark the most well-acknowledged baselines: EdgePred [34], InfoGraph [82], GPT-GNN[43], AttrMask & ContextPred[42], GraphLoG[101], G-{Contextual, Motif}[77], GraphCL[104], JOAO[103].

Our method. GraphMVP has two key factors: i) masking ratio (M) and ii) number of conformers for each molecule (C). We set $M = 0.15$ and $C = 5$ by default, and will explore their effects in the following ablation studies in Section 4.3. For EBM-NCE loss, we adopt the empirical distribution for noise distribution. For Equation (8), we pick the empirically optimal generative and contrastive 2D SSL method: that is AttrMask for GraphMVP-G and ContextPred for GraphMVP-C.

The main results on 8 molecular property prediction tasks are listed in Table 1. We observe that the performance of GraphMVP is significantly better than the random initialized one, and the average performance outperforms the existing SSL methods by a large margin. In addition, GraphMVP-G and GraphMVP-C consistently improve the performance, supporting the claim: **3D geometry is complementary to the 2D topology**. GraphMVP leverages the information between 3D geometry and 2D topology, and 2D SSL plays the role as regularizer to extract more 2D topological information; they are extracting different perspectives of information and are indeed complementary to each other.

4.3 ABLATION STUDY: THE EFFECT OF MASKING RATIO AND NUMBER OF CONFORMERS

We analyze the effects of masking ratio M and the number of conformers C in GraphMVP. In Table 1, we set the M as 0.15 since it has been widely used in existing SSL methods [42, 103, 104], and

Table 2: Ablation of masking ratio M , $C \equiv 5$.

M	GraphMVP	GraphMVP-G	GraphMVP-C
0	71.12	72.15	72.66
0.15	71.60	72.76	73.08
0.30	71.79	72.91	73.17

Table 3: Ablation of # conformer C , $M \equiv 0.15$.

C	GraphMVP	GraphMVP-G	GraphMVP-C
1	71.61	72.80	72.46
5	71.60	72.76	73.08
10	72.20	72.59	73.09
20	72.39	73.00	73.02

C is set to 5, which we will explain below. We explore on the range of $M \in \{0, 0.15, 0.3\}$ and $C \in \{1, 5, 10, 20\}$, and report the average performance. The complete results are in Appendix G.2.

As seen in Table 2, the improvement is more obvious from $M = 0$ (raw graph) to $M = 0.15$ than from $M = 0.15$ to $M = 0.3$. This can be explained that subgraph masking with larger ratio will make the SSL tasks more challenging, especially comparing to the raw graph ($M = 0$).

Table 3 shows the effect for C . We observe that the performance is generally better when adding more conformers, but will reach a plateau above certain thresholds. This observation matches with previous findings [5]: adding more conformers to augment the representation learning is not as helpful as expected; while we conclude that adding more conformers can be beneficial with little improvement. One possible reason is, when generating the dataset, we are sampling top- C conformers with highest possibility and lowest energy. In other words, top-5 conformers are sufficient to cover the most conformers with equilibrium state (over 80%), and the effect of larger C is thus modest.

To sum up, adding more conformers might be helpful, but the computation cost can grow linearly with the increase in dataset size. On the other hand, enlarging the masking ratio will not induce extra cost, yet the performance is slightly better. Therefore, we would encourage tuning masking ratios prior to trying a larger number of conformers from the perspective of efficiency and effectiveness.

4.4 ABLATION STUDY: THE EFFECT OF OBJECTIVE FUNCTION

In Section 3, we introduce a new contrastive learning objective family called EBM-NCE, and we take either InfoNCE and EBM-NCE as the contrastive SSL. For the generative SSL task, we propose a novel objective function called variational representation reconstruction (VRR) in Equation (6). As discussed in Section 3.3, stochasticity is important for GraphMVP since it can capture the conformer distribution for each 2D molecular graph. To verify this, we add an ablation study on *representation reconstruction (RR)* by removing stochasticity in VRR. Thus, here we deploy a comprehensive ablation study to explore the effect for each individual objective function (InfoNCE, EBM-NCE, VRR and RR), followed by the pairwise combinations between them.

Table 4: Ablation on the objective function.

GraphMVP Loss	Contrastive	Generative	Avg
Random			67.21
InfoNCE only	✓		68.85
EBM-NCE only	✓		70.15
VRR only		✓	69.29
RR only		✓	68.89
InfoNCE + VRR	✓	✓	70.67
EBM-NCE + VRR	✓	✓	71.69
InfoNCE + RR	✓	✓	70.60
EBM-NCE + RR	✓	✓	70.94

The results in Table 4 give certain constructive insights as follows: (1) Each individual SSL objective function (middle block) can lead to better performance. This strengthens the claim that adding 3D information is helpful for 2D representation learning. (2) According to the combination of those SSL objective functions (bottom block), adding both contrastive and generative SSL can consistently improve the performance. This verifies our claim that conducting SSL at both the inter-data and intra-data level is beneficial. (3) We can see VRR is consistently better than RR on all settings, which verifies that stochasticity is an important factor in modeling 3D conformers for molecules.

4.5 BROADER RANGE OF DOWNSTREAM TASKS

The 8 binary downstream tasks discussed so far have been widely applied in the graph SSL research line on molecules [42, 103, 104], but there are more tasks where the 3D conformers can be helpful. Here we test 4 extra regression property prediction tasks and 2 drug-target affinity tasks.

About the dataset statistics, more detailed information can be found in Appendix F, and we may as well briefly describe the affinity task here. Drug-target affinity (DTA) is a crucial task [70, 71, 96] in drug discovery, where it models both the molecular drugs and target proteins, with the goal to predict

Table 5: Results for four molecular property prediction tasks (regression) and two DTA tasks (regression). We report the mean RMSE of 3 seeds with scaffold splitting for molecular property downstream tasks, and mean MSE for 3 seeds with random splitting on DTA tasks. For GraphMVP, we set $M = 0.15$ and $C = 5$. The best performance for each task is marked in **bold**. We omit the std here since they are very small and indistinguishable. For complete results, please check Appendix G.4.

Pre-training	Molecular Property Prediction					Drug-Target Affinity		
	ESOL	Lipo	Malaria	CEP	Avg	Davis	KIBA	Avg
-	1.178	0.744	1.127	1.254	1.0756	0.286	0.206	0.2459
AM	1.112	0.730	1.119	1.256	1.0542	0.291	0.203	0.2476
CP	1.196	0.702	1.101	1.243	1.0606	0.279	0.198	0.2382
JOAO	1.120	0.708	1.145	1.293	1.0663	0.281	0.196	0.2387
GraphMVP	1.091	0.718	1.114	1.236	1.0397	0.280	0.178	0.2286
GraphMVP-G	1.064	0.691	1.106	1.228	1.0221	0.274	0.175	0.2248
GraphMVP-C	1.029	0.681	1.097	1.244	1.0128	0.276	0.168	0.2223

their affinity scores. One recent work [66] is modeling the molecular drugs with 2D GNN and target protein (as an amino-acid sequence) with convolution neural network (CNN). We adopt this setting by pre-training the 2D GNN using GraphMVP. As illustrated in Table 5, the consistent performance gain verifies the effectiveness of our proposed GraphMVP.

4.6 CASE STUDY

We investigate how GraphMVP helps when the task objectives are challenging with respect to the 2D topology but straightforward using 3D geometry (as shown in Figure 2). We therefore design two case studies to testify how GraphMVP transfers knowledge from 3D geometry into the 2D representation.

The first case study is *3D Diameter Prediction*. For molecules, usually, the longer the 2D diameter is, the larger the 3D diameter (largest atomic pairwise l2 distance). However, this does not always hold, and we are interested in using the 2D graph to predict the 3D diameter. The second case study is *Long-Range Donor-Acceptor Detection*. Molecules possess a special geometric structure called donor-acceptor bond, and we want to use 2D molecular graph to detect this special structure. We validate that GraphMVP consistently brings improvements on these 2 case studies, and provide more detailed discussions and interpretations in Appendix G.6.

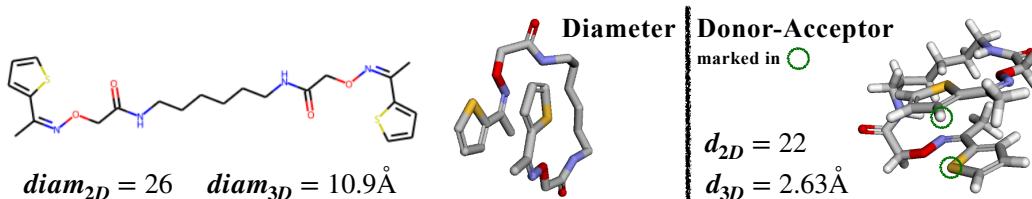


Figure 2: We select the molecules whose properties can be easily resolved via 3D but not 2D. The randomly initialised 2D GNN achieves accuracy of 38.9 ± 0.8 and 77.9 ± 1.1 , respectively. The GraphMVP pre-trained ones obtain scores of 42.3 ± 1.3 and 81.5 ± 0.4 , outperforming all the precedents in Section 4.2. We plot cases where random initialization fails but GraphMVP is correct.

5 THEORETICAL INSIGHTS

In this section, we provide the mathematical insights behind GraphMVP. We will first discuss both contrastive and generative SSL methods (Sections 3.2 and 3.3) are maximizing the mutual information (MI) and then how the 3D geometry, as privileged information, can help 2D representation learning.

5.1 MAXIMIZING MUTUAL INFORMATION

Mutual information (MI) measures the non-linear dependence [7] between two random variables: the larger MI, the stronger dependence between the variables. Therefore for GraphMVP, we can interpret it as maximizing MI between 2D and 3D views: to obtain a more robust 2D/3D representation

by sharing more information with its 3D/2D counterparts. This is also consistent with the sample complexity theory [3, 20, 26] where SSL as functional regularizer can reduce the uncertainty in representation learning. We first derive a lower bound for MI (see derivations in Appendix C), and the corresponding objective function \mathcal{L}_{MI} is

$$I(X; Y) \geq \mathcal{L}_{\text{MI}} = \frac{1}{2} \mathbb{E}_{p(\mathbf{x}, \mathbf{y})} [\log p(\mathbf{y}|\mathbf{x}) + \log p(\mathbf{x}|\mathbf{y})]. \quad (9)$$

Contrastive Self-Supervised Learning. InfoNCE was initialized proposed to maximize the MI directly [69]. Here in GraphMVP, EBM-NCE estimates the conditional likelihood in Equation (9) using EBM, and solves it with NCE [32]. As a result, EBM-NCE can also be seen as maximizing MI between 2D and 3D views. The detailed derivations can be found in Appendix D.2.

Generative Self-Supervised Learning. One alternative solution is to use a variational lower bound to approximate the conditional log-likelihood terms in Equation (9). Then we can follow the same pipeline in Section 3.3, ending up with the surrogate objective, *i.e.*, VRR in Equation (6).

5.2 3D GEOMETRY AS PRIVILEGED INFORMATION

We show the theoretical insights from privileged information that motivate GraphMVP. We start by considering a supervised learning setting where $(\mathbf{u}_i, \mathbf{l}_i)$ is a feature-label pair and \mathbf{u}_i^* is the privileged information [88, 89]. The privileged information is defined to be additional information about the input $(\mathbf{u}_i, \mathbf{l}_i)$ in order to support the prediction. For example, \mathbf{u}_i could be some CT images of a particular disease, \mathbf{l}_i could be the label of the disease and \mathbf{u}_i^* is the medical report from a doctor. VC theory [87, 88] characterizes the learning speed of an algorithm from the capacity of the algorithm and the amount of training data. Considering a binary classifier f from a function class \mathcal{F} with finite VC-dimension $\text{VCD}(\mathcal{F})$. With probability $1 - \delta$, the expected error is upper bounded by

$$R(f) \leq R_n(f) + \mathcal{O}\left(\left(\frac{\text{VCD}(\mathcal{F}) - \log \delta}{n}\right)^\beta\right) \quad (10)$$

where $R_n(f)$ denotes the training error and n is the number of training samples. When the training data is separable, then $R_n(f)$ will diminish to zero and β is equal to 1. When the training data is non-separable, β is $\frac{1}{2}$. Therefore, the rate of convergence for the separable case is of order $1/n$. In contrast, the rate for the non-separable case is of order $1/\sqrt{n}$. We note that such a difference is huge, since the same order of bounds require up to 100 training samples versus 10,000 samples. Privileged information makes the training data separable such that the learning can be more efficient. Connecting the results to GraphMVP, we notice that the 3D geometric information of molecules can be viewed as a form of privileged information, since 3D information can effectively make molecules more separable for some properties [54, 58, 79]. Besides, privileged information is only used in training, and it well matches our usage of 3D geometry for pre-training. In fact, using 3D structures as privileged information has been already shown quite useful in protein classification [89], which serves as a strong evidence to justify the effectiveness of 3D information in graph SSL pre-training.

6 CONCLUSION AND FUTURE WORK

In this work, we provide a very general framework, coined GraphMVP. From the domain perspective, GraphMVP (1) is the first to incorporate 3D information for augmenting 2D graph representation learning and (2) is able to take advantages of 3D conformers by considering stochasticity in modeling. From the aspect of technical novelties, GraphMVP brings following insights when introducing 2 SSL tasks: (1) Following Equation (9), GraphMVP proposes EBM-NCE and VRR, where they are modeling the conditional distributions using EBM and variational distribution respectively. (2) EBM-NCE is similar to JSE, while we start with a different direction for theoretical intuition, yet EBM opens another promising venue in this area. (3) VRR, as a generative SSL method, is able to alleviate the potential issues in molecule generation [25, 106]. (4) Ultimately, GraphMVP combines both contrastive SSL (InfoNCE or EBM-NCE) and generative SSL (VRR) for objective function. Both empirical results (solid performance improvements on 14 downstream datasets) and theoretical analysis can strongly support the above domain and technical contributions.

We want to emphasize that GraphMVP is model-agnostic and has the potential to be expanded to many other low-data applications. This motivates broad directions for future exploration, including but not limited to: (1) More powerful 2D and 3D molecule representation methods. (2) Different application domain other than small molecules, *e.g.*, large molecules like proteins.

REPRODUCIBILITY STATEMENT

To ensure the reproducibility of the empirical results, we include our code base in the supplementary material, which contains: instructions for installing conda virtual environment, data preprocessing scripts, and training scripts. Our code is available on [GitHub](#) for reproducibility. Complete derivations of equations and clear explanations are given in Appendices C to E.

ACKNOWLEDGEMENT

This project is supported by the Natural Sciences and Engineering Research Council (NSERC) Discovery Grant, the Canada CIFAR AI Chair Program, collaboration grants between Microsoft Research and Mila, Samsung Electronics Co., Ltd., Amazon Faculty Research Award, Tencent AI Lab Rhino-Bird Gift Fund and a NRC Collaborative R&D Project (AI4D-CORE-06). This project was also partially funded by IVADO Fundamental Research Project grant PRF-2019-3583139727.

REFERENCES

- [1] Moayad Alnammi, Shengchao Liu, Spencer S Ericksen, Gene E Ananiev, Andrew F Voter, Song Guo, James L Keck, F Michael Hoffmann, Scott A Wildman, and Anthony Gitter. Evaluating scalable supervised learning for synthesize-on-demand chemical libraries. 2021. [18](#)
- [2] Michael Arbel, Liang Zhou, and Arthur Gretton. Generalized energy based models. *arXiv preprint arXiv:2003.05033*, 2020. [23](#), [24](#)
- [3] Sanjeev Arora, Hrishikesh Khandeparkar, Mikhail Khodak, Orestis Plevrakis, and Nikunj Saunshi. A theoretical analysis of contrastive unsupervised representation learning. *arXiv preprint arXiv:1902.09229*, 2019. [4](#), [9](#)
- [4] Simon Axelrod and Rafael Gomez-Bombarelli. Geom: Energy-annotated molecular conformations for property prediction and molecular generation. *arXiv preprint arXiv:2006.05531*, 2020. [2](#), [5](#), [6](#), [19](#)
- [5] Simon Axelrod and Rafael Gomez-Bombarelli. Molecular machine learning with conformer ensembles. *arXiv preprint arXiv:2012.08452*, 2020. [7](#)
- [6] Philip Bachman, R Devon Hjelm, and William Buchwalter. Learning representations by maximizing mutual information across views. *arXiv preprint arXiv:1906.00910*, 2019. [2](#)
- [7] Mohamed Ishmael Belghazi, Aristide Baratin, Sai Rajeshwar, Sherjil Ozair, Yoshua Bengio, Aaron Courville, and Devon Hjelm. Mutual information neural estimation. In *International Conference on Machine Learning*, pages 531–540. PMLR, 2018. [2](#), [5](#), [8](#), [26](#)
- [8] Tom B Brown, Benjamin Mann, Nick Ryder, Melanie Subbiah, Jared Kaplan, Prafulla Dhariwal, Arvind Neelakantan, Pranav Shyam, Girish Sastry, Amanda Askell, et al. Language models are few-shot learners. *arXiv preprint arXiv:2005.14165*, 2020. [17](#)
- [9] Mathilde Caron, Ishan Misra, Julien Mairal, Priya Goyal, Piotr Bojanowski, and Armand Joulin. Unsupervised learning of visual features by contrasting cluster assignments. *arXiv preprint arXiv:2006.09882*, 2020. [17](#)
- [10] Ting Chen, Simon Kornblith, Mohammad Norouzi, and Geoffrey Hinton. A simple framework for contrastive learning of visual representations. In *International conference on Machine Learning*, pages 1597–1607, 2020. [4](#), [17](#)
- [11] Xi Chen, Yan Duan, Rein Houthooft, John Schulman, Ilya Sutskever, and Pieter Abbeel. Infogan: Interpretable representation learning by information maximizing generative adversarial nets. In *Proceedings of the 30th International Conference on Neural Information Processing Systems*, pages 2180–2188, 2016. [4](#)
- [12] Xinlei Chen and Kaiming He. Exploring simple siamese representation learning. In *Proceedings of the IEEE/CVF Conference on Computer Vision and Pattern Recognition*, pages 15750–15758, 2021. [5](#), [17](#), [26](#)
- [13] Gabriele Corso, Luca Cavalleri, Dominique Beaini, Pietro Liò, and Petar Veličković. Principal neighbourhood aggregation for graph nets. *arXiv preprint arXiv:2004.05718*, 2020. [18](#), [19](#)
- [14] Mindy I Davis, Jeremy P Hunt, Sanna Herrgard, Pietro Ciceri, Lisa M Wodicka, Gabriel Pallares, Michael Hocker, Daniel K Treiber, and Patrick P Zarrinkar. Comprehensive analysis of kinase inhibitor selectivity. *Nature biotechnology*, 29(11):1046–1051, 2011. [28](#)

- [15] John S Delaney. Esol: estimating aqueous solubility directly from molecular structure. *Journal of chemical information and computer sciences*, 44(3):1000–1005, 2004. [27](#)
- [16] Mehmet F Demirel, Shengchao Liu, Siddhant Garg, and Yingyu Liang. An analysis of attentive walk-aggregating graph neural networks. *arXiv preprint arXiv:2110.02667*, 2021. [18](#)
- [17] Jacob Devlin, Ming-Wei Chang, Kenton Lee, and Kristina Toutanova. Bert: Pre-training of deep bidirectional transformers for language understanding. *arXiv preprint arXiv:1810.04805*, 2018. [1, 17](#)
- [18] Laurent Dinh, Jascha Sohl-Dickstein, and Samy Bengio. Density estimation using real nvp. *arXiv preprint arXiv:1605.08803*, 2016. [4](#)
- [19] Yilun Du, Shuang Li, Joshua Tenenbaum, and Igor Mordatch. Improved contrastive divergence training of energy based models. *arXiv preprint arXiv:2012.01316*, 2020. [22, 24](#)
- [20] Dumitru Erhan, Aaron Courville, Yoshua Bengio, and Pascal Vincent. Why does unsupervised pre-training help deep learning? In *Proceedings of the thirteenth international conference on artificial intelligence and statistics*, pages 201–208. JMLR Workshop and Conference Proceedings, 2010. [9](#)
- [21] Yin Fang, Qiang Zhang, Haihong Yang, Xiang Zhuang, Shumin Deng, Wen Zhang, Ming Qin, Zhuo Chen, Xiaohui Fan, and Huajun Chen. Molecular contrastive learning with chemical element knowledge graph. *arXiv preprint arXiv:2112.00544*, 2021. [19](#)
- [22] Elizabeth H Finn, Gianluca Pegoraro, Sigal Shachar, and Tom Misteli. Comparative analysis of 2d and 3d distance measurements to study spatial genome organization. *Methods*, 123:47–55, 2017. [30](#)
- [23] Fabian B Fuchs, Daniel E Worrall, Volker Fischer, and Max Welling. Se (3)-transformers: 3d roto-translation equivariant attention networks. *arXiv preprint arXiv:2006.10503*, 2020. [18, 19](#)
- [24] Francisco-Javier Gamo, Laura M Sanz, Jaume Vidal, Cristina De Cozar, Emilio Alvarez, Jose-Luis Lavandera, Dana E Vanderwall, Darren VS Green, Vinod Kumar, Samiul Hasan, et al. Thousands of chemical starting points for antimalarial lead identification. *Nature*, 465(7296):305, 2010. [28](#)
- [25] Wenhao Gao and Connor W Coley. The synthesizability of molecules proposed by generative models. *Journal of chemical information and modeling*, 60(12):5714–5723, 2020. [9](#)
- [26] Siddhant Garg and Yingyu Liang. Functional regularization for representation learning: A unified theoretical perspective. *arXiv preprint arXiv:2008.02447*, 2020. [9](#)
- [27] Anna Gaulton, Louisa J Bellis, A Patricia Bento, Jon Chambers, Mark Davies, Anne Hersey, Yvonne Light, Shaun McGlinchey, David Michalovich, Bissan Al-Lazikani, et al. ChEMBL: a large-scale bioactivity database for drug discovery. *Nucleic acids research*, 40(D1):D1100–D1107, 2012. [27](#)
- [28] Kaitlyn M Gayvert, Neel S Madhukar, and Olivier Elemento. A data-driven approach to predicting successes and failures of clinical trials. *Cell chemical biology*, 23(10):1294–1301, 2016. [27](#)
- [29] Justin Gilmer, Samuel S Schoenholz, Patrick F Riley, Oriol Vinyals, and George E Dahl. Neural message passing for quantum chemistry. In *International Conference on Machine Learning*, pages 1263–1272. PMLR, 2017. [1, 18](#)
- [30] Ian Goodfellow, Jean Pouget-Abadie, Mehdi Mirza, Bing Xu, David Warde-Farley, Sherjil Ozair, Aaron Courville, and Yoshua Bengio. Generative adversarial nets. *Advances in neural information processing systems*, 27, 2014. [4](#)
- [31] Jean-Bastien Grill, Florian Strub, Florent Altché, Corentin Tallec, Pierre H Richemond, Elena Buchatskaya, Carl Doersch, Bernardo Avila Pires, Zhaohan Daniel Guo, Mohammad Gheshlaghi Azar, et al. Bootstrap your own latent: A new approach to self-supervised learning. *arXiv preprint arXiv:2006.07733*, 2020. [5, 26](#)
- [32] Michael Gutmann and Aapo Hyvärinen. Noise-contrastive estimation: A new estimation principle for unnormalized statistical models. In *Proceedings of the thirteenth international conference on artificial intelligence and statistics*, pages 297–304. JMLR Workshop and Conference Proceedings, 2010. [9, 22](#)
- [33] Johannes Hachmann, Roberto Olivares-Amaya, Sule Atahan-Evrak, Carlos Amador-Bedolla, Roel S Sánchez-Carrera, Aryeh Gold-Parker, Leslie Vogt, Anna M Brockway, and Alán Aspuru-Guzik. The harvard clean energy project: large-scale computational screening and design of organic photovoltaics on the world community grid. *The Journal of Physical Chemistry Letters*, 2(17):2241–2251, 2011. [27](#)

- [34] William L Hamilton, Rex Ying, and Jure Leskovec. Inductive representation learning on large graphs. In *Advances in Neural Information Processing Systems, NeurIPS*, 2017. [2](#), [6](#), [17](#)
- [35] Kaveh Hassani and Amir Hosein Khasahmadi. Contrastive multi-view representation learning on graphs. In *International Conference on Machine Learning*, pages 4116–4126. PMLR, 2020. [4](#)
- [36] Paul CD Hawkins. Conformation generation: the state of the art. *Journal of Chemical Information and Modeling*, 57(8):1747–1756, 2017. [2](#), [19](#)
- [37] Kaiming He, Haoqi Fan, Yuxin Wu, Saining Xie, and Ross Girshick. Momentum contrast for unsupervised visual representation learning. In *Proceedings of the IEEE/CVF Conference on Computer Vision and Pattern Recognition*, pages 9729–9738, 2020. [4](#), [17](#)
- [38] Irina Higgins, Loic Matthey, Arka Pal, Christopher Burgess, Xavier Glorot, Matthew Botvinick, Shakir Mohamed, and Alexander Lerchner. beta-vae: Learning basic visual concepts with a constrained variational framework. In *International Conference on Learning Representations*, 2017. [1](#), [26](#)
- [39] Maya Hirohara, Yutaka Saito, Yuki Koda, Kengo Sato, and Yasubumi Sakakibara. Convolutional neural network based on SMILES representation of compounds for detecting chemical motif. *BMC bioinformatics*, 19(19):83–94, 2018. [19](#)
- [40] R Devon Hjelm, Alex Fedorov, Samuel Lavoie-Marchildon, Karan Grewal, Phil Bachman, Adam Trischler, and Yoshua Bengio. Learning deep representations by mutual information estimation and maximization. *arXiv preprint arXiv:1808.06670*, 2018. [24](#)
- [41] Qianjiang Hu, Xiao Wang, Wei Hu, and Guo-Jun Qi. Adco: Adversarial contrast for efficient learning of unsupervised representations from self-trained negative adversaries. In *Proceedings of the IEEE/CVF Conference on Computer Vision and Pattern Recognition*, pages 1074–1083, 2021. [24](#)
- [42] Weihua Hu, Bowen Liu, Joseph Gomes, Marinka Zitnik, Percy Liang, Vijay Pande, and Jure Leskovec. Strategies for pre-training graph neural networks. In *International Conference on Learning Representations, ICLR*, 2020. [1](#), [2](#), [4](#), [6](#), [7](#), [17](#), [18](#)
- [43] Ziniu Hu, Yuxiao Dong, Kuansan Wang, Kai-Wei Chang, and Yizhou Sun. Gpt-gnn: Generative pre-training of graph neural networks. In *ACM SIGKDD International Conference on Knowledge Discovery & Data Mining, KDD*, pages 1857–1867, 2020. [2](#), [6](#), [17](#)
- [44] Dejun Jiang, Zhenxing Wu, Chang-Yu Hsieh, Guangyong Chen, Ben Liao, Zhe Wang, Chao Shen, Dongsheng Cao, Jian Wu, and Tingjun Hou. Could graph neural networks learn better molecular representation for drug discovery? a comparison study of descriptor-based and graph-based models. *Journal of cheminformatics*, 13(1):1–23, 2021. [18](#)
- [45] John Jumper, Richard Evans, Alexander Pritzel, Tim Green, Michael Figurnov, Olaf Ronneberger, Kathryn Tunyasuvunakool, Russ Bates, Augustin Žídek, Anna Potapenko, et al. Highly accurate protein structure prediction with alphafold. *Nature*, pages 1–11, 2021. [18](#), [19](#)
- [46] Ramandeep Kaur, Fabio Possanza, Francesca Limosani, Stefan Bauroth, Robertino Zanoni, Timothy Clark, Giorgio Arrigoni, Pietro Tagliatesta, and Dirk M Guldi. Understanding and controlling short-and long-range electron/charge-transfer processes in electron donor–acceptor conjugates. *Journal of the American Chemical Society*, 142(17):7898–7911, 2020. [30](#)
- [47] Prannay Khosla, Piotr Teterwak, Chen Wang, Aaron Sarna, Yonglong Tian, Phillip Isola, Aaron Maschinot, Ce Liu, and Dilip Krishnan. Supervised contrastive learning. *arXiv preprint arXiv:2004.11362*, 2020. [24](#)
- [48] Diederik P Kingma and Prafulla Dhariwal. Glow: generative flow with invertible 1×1 convolutions. In *Proceedings of the 32nd International Conference on Neural Information Processing Systems*, pages 10236–10245, 2018. [4](#), [25](#)
- [49] Diederik P Kingma and Max Welling. Auto-encoding variational bayes. *arXiv preprint arXiv:1312.6114*, 2013. [1](#), [4](#), [25](#)
- [50] Michael Kuhn, Ivica Letunic, Lars Juhl Jensen, and Peer Bork. The sider database of drugs and side effects. *Nucleic acids research*, 44(D1):D1075–D1079, 2015. [27](#)
- [51] Gustav Larsson, Michael Maire, and Gregory Shakhnarovich. Learning representations for automatic colorization. In *European conference on computer vision*, pages 577–593, 2016. [4](#), [25](#)

- [52] Shengchao Liu, Moayad Alnammi, Spencer S Erickson, Andrew F Voter, Gene E Ananiev, James L Keck, F Michael Hoffmann, Scott A Wildman, and Anthony Gitter. Practical model selection for prospective virtual screening. *Journal of chemical information and modeling*, 59(1):282–293, 2018. 18
- [53] Shengchao Liu, Andreea Deac, Zhaocheng Zhu, and Jian Tang. Structured multi-view representations for drug combinations. In *NeurIPS 2020 ML for Molecules Workshop*, 2020. 19
- [54] Shengchao Liu, Mehmet Furkan Demirel, and Yingyu Liang. N-gram graph: Simple unsupervised representation for graphs, with applications to molecules. *arXiv preprint arXiv:1806.09206*, 2018. 1, 2, 9, 17, 18, 19
- [55] Shengchao Liu, Yingyu Liang, and Anthony Gitter. Loss-balanced task weighting to reduce negative transfer in multi-task learning. In *Proceedings of the AAAI conference on artificial intelligence*, volume 33, pages 9977–9978, 2019. 18
- [56] Shengchao Liu, Meng Qu, Zuobai Zhang, Huiyu Cai, and Jian Tang. Structured multi-task learning for molecular property prediction. *arXiv preprint arXiv:2203.04695*, 2022. 19
- [57] Xiao Liu, Fanjin Zhang, Zhenyu Hou, Li Mian, Zhaoyu Wang, Jing Zhang, and Jie Tang. Self-supervised learning: Generative or contrastive. *IEEE Transactions on Knowledge and Data Engineering*, 2021. 2, 17, 21
- [58] Yi Liu, Limei Wang, Meng Liu, Xuan Zhang, Bora Oztekin, and Shuiwang Ji. Spherical message passing for 3d graph networks. *arXiv preprint arXiv:2102.05013*, 2021. 1, 2, 9, 17, 18, 19
- [59] Yixin Liu, Shirui Pan, Ming Jin, Chuan Zhou, Feng Xia, and Philip S Yu. Graph self-supervised learning: A survey. *arXiv preprint arXiv:2103.00111*, 2021. 2, 6, 17, 21, 24
- [60] Yu-Shen Liu, Qi Li, Guo-Qin Zheng, Karthik Ramani, and William Benjamin. Using diffusion distances for flexible molecular shape comparison. *BMC bioinformatics*, 11(1):1–15, 2010. 30
- [61] Ines Filipa Martins, Ana L Teixeira, Luis Pinheiro, and Andre O Falcao. A bayesian approach to in silico blood-brain barrier penetration modeling. *Journal of chemical information and modeling*, 52(6):1686–1697, 2012. 27
- [62] RVN Melnik, A Uhlherr, J Hodgkin, and F De Hoog. Distance geometry algorithms in molecular modelling of polymer and composite systems. *Computers & Mathematics with Applications*, 45(1-3):515–534, 2003. 30
- [63] Jesse G Meyer, Shengchao Liu, Ian J Miller, Joshua J Coon, and Anthony Gitter. Learning drug functions from chemical structures with convolutional neural networks and random forests. *Journal of chemical information and modeling*, 59(10):4438–4449, 2019. 18
- [64] Andriy Mnih and Yee Whye Teh. A fast and simple algorithm for training neural probabilistic language models. *arXiv preprint arXiv:1206.6426*, 2012. 23
- [65] Gerry P Moss. Basic terminology of stereochemistry (iupac recommendations 1996). *Pure and applied chemistry*, 68(12):2193–2222, 1996. 2
- [66] Thin Nguyen, Hang Le, and Svetha Venkatesh. Graphda: prediction of drug–target binding affinity using graph convolutional networks. *BioRxiv*, page 684662, 2019. 8
- [67] Didrik Nielsen, Priyank Jaini, Emiel Hoogeboom, Ole Winther, and Max Welling. Survae flows: Surjections to bridge the gap between vaes and flows. *Advances in Neural Information Processing Systems*, 33, 2020. 25
- [68] Sebastian Nowozin, Botond Cseke, and Ryota Tomioka. f-gan: Training generative neural samplers using variational divergence minimization. In *Proceedings of the 30th International Conference on Neural Information Processing Systems*, pages 271–279, 2016. 4, 24
- [69] Aaron van den Oord, Yazhe Li, and Oriol Vinyals. Representation learning with contrastive predictive coding. *arXiv preprint arXiv:1807.03748*, 2018. 4, 9, 17, 21
- [70] Hakime Öztürk, Arzucan Özgür, and Elif Ozkirimli. Deepdta: deep drug–target binding affinity prediction. *Bioinformatics*, 34(17):i821–i829, 2018. 7, 28
- [71] Tapio Pahikkala, Antti Airola, Sami Pietilä, Sushil Shakyawar, Agnieszka Szwajda, Jing Tang, and Tero Aittokallio. Toward more realistic drug–target interaction predictions. *Briefings in bioinformatics*, 16(2):325–337, 2015. 7

- [72] Lagnajit Pattanaik, Octavian-Eugen Ganea, Ian Coley, Klavs F Jensen, William H Green, and Connor W Coley. Message passing networks for molecules with tetrahedral chirality. *arXiv preprint arXiv:2012.00094*, 2020. 31
- [73] Ben Poole, Sherjil Ozair, Aaron Van Den Oord, Alex Alemi, and George Tucker. On variational bounds of mutual information. In *International Conference on Machine Learning*, pages 5171–5180. PMLR, 2019. 24
- [74] Zhuoran Qiao, Anders S Christensen, Frederick R Manby, Matthew Welborn, Anima Anandkumar, and Thomas F Miller III. Unite: Unitary n-body tensor equivariant network with applications to quantum chemistry. *arXiv preprint arXiv:2105.14655*, 2021. 19
- [75] Bharath Ramsundar, Steven Kearnes, Patrick Riley, Dale Webster, David Konerding, and Vijay Pande. Massively multitask networks for drug discovery. *arXiv preprint arXiv:1502.02072*, 2015. 18
- [76] Sebastian G Rohrer and Knut Baumann. Maximum unbiased validation (muv) data sets for virtual screening based on pubchem bioactivity data. *Journal of chemical information and modeling*, 49(2):169–184, 2009. 27
- [77] Yu Rong, Yatao Bian, Tingyang Xu, Weiyang Xie, Ying Wei, Wenbing Huang, and Junzhou Huang. Self-supervised graph transformer on large-scale molecular data. In *Advances in Neural Information Processing Systems, NeurIPS*, 2020. 6, 17, 28
- [78] Victor Garcia Satorras, Emiel Hoogeboom, and Max Welling. E (n) equivariant graph neural networks. *arXiv preprint arXiv:2102.09844*, 2021. 18, 19
- [79] Kristof T Schütt, Pieter-Jan Kindermans, Huziel E Sauceda, Stefan Chmiela, Alexandre Tkatchenko, and Klaus-Robert Müller. Schnet: A continuous-filter convolutional neural network for modeling quantum interactions. *arXiv preprint arXiv:1706.08566*, 2017. 1, 2, 6, 9, 17, 18, 19
- [80] Yang Song and Diederik P Kingma. How to train your energy-based models. *arXiv preprint arXiv:2101.03288*, 2021. 22, 23, 24
- [81] Yang Song, Jascha Sohl-Dickstein, Diederik P Kingma, Abhishek Kumar, Stefano Ermon, and Ben Poole. Score-based generative modeling through stochastic differential equations. *arXiv preprint arXiv:2011.13456*, 2020. 22, 24
- [82] Fan-Yun Sun, Jordan Hoffmann, Vikas Verma, and Jian Tang. Infograph: Unsupervised and semi-supervised graph-level representation learning via mutual information maximization. In *International Conference on Learning Representations, ICLR*, 2020. 1, 2, 4, 6, 17, 24
- [83] Jing Tang, Agnieszka Szwajda, Sushil Shakyawar, Tao Xu, Petteri Hintsanen, Krister Wennerberg, and Tero Aittokallio. Making sense of large-scale kinase inhibitor bioactivity data sets: a comparative and integrative analysis. *Journal of Chemical Information and Modeling*, 54(3):735–743, 2014. 28
- [84] Yuandong Tian, Xinlei Chen, and Surya Ganguli. Understanding self-supervised learning dynamics without contrastive pairs. *arXiv preprint arXiv:2102.06810*, 2021. 26
- [85] Tox21 Data Challenge. Tox21 data challenge 2014. <https://tripod.nih.gov/tox21/challenge/>, 2014. 27
- [86] Michael Tschannen, Josip Djolonga, Paul K Rubenstein, Sylvain Gelly, and Mario Lucic. On mutual information maximization for representation learning. *arXiv preprint arXiv:1907.13625*, 2019. 2
- [87] Vladimir Vapnik. *The nature of statistical learning theory*. Springer science & business media, 2013. 9
- [88] Vladimir Vapnik, Rauf Izmailov, et al. Learning using privileged information: similarity control and knowledge transfer. *J. Mach. Learn. Res.*, 16(1):2023–2049, 2015. 2, 9
- [89] Vladimir Vapnik and Akshay Vashist. A new learning paradigm: Learning using privileged information. *Neural networks*, 22(5-6):544–557, 2009. 2, 9
- [90] Petar Veličković, William Fedus, William L Hamilton, Pietro Liò, Yoshua Bengio, and R Devon Hjelm. Deep graph infomax. *arXiv preprint arXiv:1809.10341*, 2018. 1, 2, 17
- [91] Pascal Vincent, Hugo Larochelle, Yoshua Bengio, and Pierre-Antoine Manzagol. Extracting and composing robust features with denoising autoencoders. In *Proceedings of the 25th international conference on Machine learning*, pages 1096–1103, 2008. 1
- [92] Hanchen Wang, Qi Liu, Xiangyu Yue, Joan Lasenby, and Matthew J. Kusner. Unsupervised point cloud pre-training via view-point occlusion, completion. In *ICCV*, 2021. 17

- [93] Tongzhou Wang and Phillip Isola. Understanding contrastive representation learning through alignment and uniformity on the hypersphere. In *International Conference on Machine Learning, ICML*, 2020. 1, 4, 17, 21
- [94] Yingheng Wang, Yaosen Min, Xin Chen, and Ji Wu. Multi-view graph contrastive representation learning for drug-drug interaction prediction. In *Proceedings of the Web Conference 2021*, pages 2921–2933, 2021. 19
- [95] David Weininger. Smiles, a chemical language and information system. 1. introduction to methodology and encoding rules. *Journal of chemical information and computer sciences*, 28(1):31–36, 1988. 19
- [96] Ming Wen, Zhimin Zhang, Shaoyu Niu, Haozhi Sha, Ruihan Yang, Yonghuan Yun, and Hongmei Lu. Deep-learning-based drug-target interaction prediction. *Journal of proteome research*, 16(4):1401–1409, 2017. 7
- [97] Lirong Wu, Haitao Lin, Zhangyang Gao, Cheng Tan, Stan Li, et al. Self-supervised on graphs: Contrastive, generative, or predictive. *arXiv preprint arXiv:2105.07342*, 2021. 2, 6, 17, 21, 24
- [98] Zhenqin Wu, Bharath Ramsundar, Evan N Feinberg, Joseph Gomes, Caleb Geniesse, Aneesh S Pappu, Karl Leswing, and Vijay Pande. Moleculenet: a benchmark for molecular machine learning. *Chemical science*, 9(2):513–530, 2018. 19, 27, 28
- [99] Yaochen Xie, Zhao Xu, Jingtun Zhang, Zhengyang Wang, and Shuiwang Ji. Self-supervised learning of graph neural networks: A unified review. *arXiv preprint arXiv:2102.10757*, 2021. 2, 6, 17, 21, 24
- [100] Keyulu Xu, Weihua Hu, Jure Leskovec, and Stefanie Jegelka. How powerful are graph neural networks? *arXiv preprint arXiv:1810.00826*, 2018. 6, 18
- [101] Minghao Xu, Hang Wang, Bingbing Ni, Hongyu Guo, and Jian Tang. Self-supervised graph-level representation learning with local and global structure. In *International Conference on Machine Learning, ICML*, 2021. 6, 17, 28
- [102] Kevin Yang, Kyle Swanson, Wengong Jin, Connor Coley, Philipp Eiden, Hua Gao, Angel Guzman-Perez, Timothy Hopper, Brian Kelley, Miriam Mathea, et al. Analyzing learned molecular representations for property prediction. *Journal of chemical information and modeling*, 59(8):3370–3388, 2019. 18, 19
- [103] Yuning You, Tianlong Chen, Yang Shen, and Zhangyang Wang. Graph contrastive learning automated. In *International Conference on Machine Learning, ICML*, 2021. 1, 2, 4, 6, 7, 17, 18, 28
- [104] Yuning You, Tianlong Chen, Yongduo Sui, Ting Chen, Zhangyang Wang, and Yang Shen. Graph contrastive learning with augmentations. In *Advances in Neural Information Processing Systems, NeurIPS*, 2020. 1, 2, 4, 6, 7, 17, 18
- [105] Daniel Zaharevitz. Aids antiviral screen data, 2015. 28
- [106] Alex Zhavoronkov, Yan A Ivanenkov, Alex Aliper, Mark S Veselov, Vladimir A Aladinskiy, Anastasiya V Aladinskaya, Victor A Terentiev, Daniil A Polykovskiy, Maksim D Kuznetsov, Arip Asadulaev, et al. Deep learning enables rapid identification of potent ddr1 kinase inhibitors. *Nature biotechnology*, 37(9):1038–1040, 2019. 9
- [107] Jinhua Zhu, Yingce Xia, Tao Qin, Wengang Zhou, Houqiang Li, and Tie-Yan Liu. Dual-view molecule pre-training. *arXiv preprint arXiv:2106.10234*, 2021. 19

Appendix

Table of Contents

A	Self-Supervised Learning on Molecular Graph	17
A.1	Contrastive graph SSL	17
A.2	Generative graph SSL	17
A.3	Predictive graph SSL	17
B	Molecular Graph Representation	18
B.1	2D Molecular Graph Neural Network	18
B.2	3D Molecular Graph Neural Network	18
B.3	Summary	19
C	Maximize Mutual Information	20
C.1	Formulation	20
C.2	A Lower Bound to MI	20
D	Contrastive Self-Supervised Learning	21
D.1	InfoNCE	21
D.2	EBM-NCE	22
D.3	EBM-NCE v.s. JSE and InfoNCE	24
E	Generative Self-Supervised Learning	25
E.1	Variational Molecule Reconstruction	25
E.2	Variational Representation Reconstruction	25
E.3	Variational Representation Reconstruction and Non-Contrastive SSL	26
F	Dataset Overview	27
F.1	Pre-Training Dataset Overview	27
F.2	Downstream Dataset Overview	27
G	Experiments Details	28
G.1	Self-supervised Learning Baselines	28
G.2	Ablation Study: The Effect of Masking Ratio and Number of Conformers	29
G.3	Ablation Study: Effect of Each Loss Component	29
G.4	Broader Range of Downstream Tasks: Molecular Property Prediction Prediction	30
G.5	Broader Range of Downstream Tasks: Drug-Target Affinity Prediction	30
G.6	Case Studies	30

A SELF-SUPERVISED LEARNING ON MOLECULAR GRAPH

Self-supervised learning (SSL) methods have attracted massive attention recently, trending from vision [9, 10, 12, 37, 92], language [8, 17, 69] to graph [42, 54, 82, 90, 103, 104]. In general, there are two categories of SSL: contrastive and generative, where they differ on the design of the supervised signals. Contrastive SSL realizes the supervised signals at the **inter-data** level, learning the representation by contrasting with other data points; while generative SSL focuses on reconstructing the original data at the **intra-data** level. Both venues have been widely explored [57, 59, 97, 99].

A.1 CONTRASTIVE GRAPH SSL

Contrastive graph SSL first applies transformations to construct different *views* for each graph. Each view incorporates different granularities of information, like node-, subgraph-, and graph-level. It then solves two sub-tasks simultaneously: (1) aligning the representations of views from the same data; (2) contrasting the representations of views from different data, leading to a uniformly distributed latent space [93]. The key difference among existing methods is thus the design of view constructions. InfoGraph [82, 90] contrasted the node (local) and graph (global) views. ContextPred [42] and G-Contextual [77] contrasted between node and context views. GraphCL and JOAO [103, 104] made comprehensive comparisons among four graph-level transformations and further learned to select the most effective combinations.

A.2 GENERATIVE GRAPH SSL

Generative graph SSL aims at reconstructing important structures for each graph. By so doing, it consequently learns a representation capable of encoding key ingredients of the data. EdgePred [34] and AttrMask [42] predicted the adjacency matrix and masked tokens (nodes and edges) respectively. GPT-GNN [43] reconstructed the whole graph in an auto-regressive approach.

A.3 PREDICTIVE GRAPH SSL

There are certain SSL methods specific to the molecular graph. For example, one central task in drug discovery is to find the important substructure or motif in molecules that can activate the target interactions. G-Motif [77] adopts domain knowledge to heuristically extract motifs for each molecule, and the SSL task is to make prediction on the existence of each motif. Different from contrastive and generative SSL, recent literature [97] takes this as predictive graph SSL, where the supervised signals are self-generated labels.

SSL for Molecular Graphs. Recall that all previous methods in Table 6 **merely** focus on the 2D topology. However, for science-centric tasks such as molecular property prediction, 3D geometry should be incorporated as it provides complementary and comprehensive information [58, 79]. To

Table 6: Comparison between GraphMVP and existing graph SSL methods.

SSL Pre-training	Graph View		SSL Category		
	2D Topology	3D Geometry	Generative	Contrastive	Predictive
EdgePred [34]	✓	-	✓	-	-
AttrMask [42]	✓	-	✓	-	-
GPT-GNN [43]	✓	-	✓	-	-
InfoGraph [82, 90]	✓	-	-	✓	-
ContexPred [42]	✓	-	-	✓	-
GraphLoG [101]	✓	-	-	✓	-
G-Contextual [77]	✓	-	-	✓	-
GraphCL [104]	✓	-	-	✓	-
JOAO [103]	✓	-	-	✓	-
G-Motif [77]	✓	-	-	-	✓
GraphMVP (Ours)	✓	✓	✓	✓	-

mitigate this gap, we propose GraphMVP to leverage the 3D geometry with unsupervised graph pre-training.

B MOLECULAR GRAPH REPRESENTATION

There are two main methods for molecular graph representation learning. The first one is the molecular fingerprints. It is a hashed bit vector to describe the molecular graph. There has been re-discoveries on fingerprints-based methods [1, 44, 52, 55, 63, 75], while its has one main drawback: Random forest and XGBoost are very strong learning models on fingerprints, but they fail to take benefits of the pre-training strategy.

Graph neural network (GNN) has become another mainstream modeling methods for molecular graph representation. Existing methods can be generally split into two venues: 2D GNN and 3D GNN, depending on what levels of information is considered. 2D GNN focuses on the topological structures of the graph, like the adjacency among nodes, while 3D GNN is able to model the “energy” of molecules by taking account the spatial positions of atoms.

First, we want to highlight that GraphMVP is model-agnostic, *i.e.*, it can be applied to any 2D and 3D GNN representation function, yet the specific 2D and 3D representations are not the main focus of this work. Second, we acknowledge there are a lot of advanced 3D [23, 45, 58, 78] and 2D [13, 16, 29, 54, 100, 102] representation methods. However, considering the *graph SSL literature* and *graph representation literature* (illustrated below), we adopt GIN [100] and SchNet [79] in current GraphMVP.

B.1 2D MOLECULAR GRAPH NEURAL NETWORK

The 2D representation is taking each molecule as a 2D graph, with atoms as nodes and bonds as edges, *i.e.*, $g_{2D} = (X, E)$. $X \in \mathbb{R}^{n \times d_n}$ is the atom attribute matrix, where n is the number of atoms (nodes) and d_n is the atom attribute dimension. $E \in \mathbb{R}^{m \times d_e}$ is the bond attribute matrix, where m is the number of bonds (edges) and d_m is the bond attribute dimension. Notice that here E also includes the connectivity. Then we will apply a transformation function T_{2D} on the topological graph. Given a 2D graph g_{2D} , its 2D molecular representation is:

$$h_{2D} = \text{GNN-2D}(T_{2D}(g_{2D})) = \text{GNN-2D}(T_{2D}(X, E)). \quad (11)$$

The core operation of 2D GNN is the message passing function [29], which updates the node representation based on adjacency information. We have variants depending on the design of message and aggregation functions, and we pick GIN [100] in this work.

GIN There has been a long research line on 2D graph representation learning [13, 16, 29, 54, 100, 102]. Among these, graph isomorphism network (GIN) model [100] has been widely used as the backbone model in recent graph self-supervised learning work [42, 103, 104]. Thus, we as well adopt GIN as the base model for 2D representation.

Recall each molecule is represented as a molecular graph, *i.e.*, $g_{2D} = (X, E)$, where X and E are feature matrices for atoms and bonds respectively. Then the message passing function is defined as:

$$z_i^{(k+1)} = \text{MLP}_{\text{atom}}^{(k+1)} \left(z_i^{(k)} + \sum_{j \in \mathcal{N}(i)} (z_j^{(k)} + \text{MLP}_{\text{bond}}^{(k+1)}(E_{ij})) \right), \quad (12)$$

where $z_0 = X$ and $\text{MLP}_{\text{atom}}^{(k+1)}$ and $\text{MLP}_{\text{bond}}^{(k+1)}$ are the $(l+1)$ -th MLP layers on the atom- and bond-level respectively. Repeating this for K times, and we can encode K -hop neighborhood information for each center atom in the molecular data, and we take the last layer for each node/atom representation. The graph-level molecular representation is the mean of the node representation:

$$z(\mathbf{x}) = \frac{1}{N} \sum_i z_i^{(K)} \quad (13)$$

B.2 3D MOLECULAR GRAPH NEURAL NETWORK

Recently, the 3D geometric representation learning has brought breakthrough progress in molecule modeling [23, 45, 58, 78, 79]. 3D molecular graph additionally includes spatial locations of the atoms,

which needless to be static since, in real scenarios, atoms are in continual motion on a *potential energy surface* [4]. The 3D structures at the local minima on this surface are named *molecular conformation* or *conformer*. As the molecular properties are a function of the conformer ensembles [36], this reveals another limitation of existing mainstream methods: to predict properties from a single 2D or 3D graph cannot account for this fact [4], while our proposed method can alleviate this issue to a certain extent.

For specific 3D molecular graph, it additionally includes spatial positions of the atoms. We represent each conformer as $g_{3D} = (X, R)$, where $R \in \mathbb{R}^{n \times 3}$ is the 3D-coordinate matrix, and the corresponding representation is:

$$h_{3D} = \text{GNN-3D}(T_{3D}(g_{3D})) = \text{GNN-3D}(T_{3D}(X, R)), \quad (14)$$

where R is the 3D-coordinate matrix and T_{3D} is the 3D transformation. Note that further information such as plane and torsion angles can be solved from the positions.

SchNet SchNet [79] is composed of the following key steps:

$$\begin{aligned} z_i^{(0)} &= \text{embedding}(x_i) \\ z_i^{(t+1)} &= \text{MLP}\left(\sum_{j=1}^n f(x_j^{(t-1)}, r_i, r_j)\right) \\ h_i &= \text{MLP}(z_i^{(K)}), \end{aligned} \quad (15)$$

where K is the number of hidden layers, and

$$f(x_j, r_i, r_j) = x_j \cdot e_k(r_i - r_j) = x_j \cdot \exp(-\gamma \|r_i - r_j\|_2 - \mu\|_2^2) \quad (16)$$

is the continuous-filter convolution layer, enabling the modeling of continuous positions of atoms.

We adopt SchNet for the following reasons. (1) SchNet is a very strong geometric representation method after *fair* benchmarking. (2) SchNet can be trained more efficiently, comparing to the other recent 3D models. To support these two points, we make a comparison among the most recent 3D geometric models [23, 58, 78] on QM9 dataset. QM9 [98] is a molecule dataset approximating 12 thermodynamic properties calculated by density functional theory (DFT) algorithm. Notice: UNiTE [74] is the state-of-the-art 3D GNN, but it requires a commercial software for feature extraction, thus we exclude it for now.

Table 7: Reproduced MAE on QM9. 100k for training, 17,748 for val, 13,083 for test. The last column is the approximated running time.

	alpha	gap	homo	lumo	mu	cv	g298	h298	r2	u298	u0	zpve	time
SchNet [79]	0.077	50	32	26	0.030	0.032	15	14	0.122	14	14	1.751	3h
SE(3)-Trans [23]	0.143	59	36	36	0.052	0.068	68	72	1.969	68	74	5.517	50h
EGNN [78]	0.075	49	29	26	0.030	0.032	11	10	0.076	10	10	1.562	24h
SphereNet [58]	0.054	41	22	19	0.028	0.027	10	8	0.295	8	8	1.401	50h

Table 7 shows that, under a fair comparison (w.r.t. data splitting, seed, cuda version, etc), SchNet can reach pretty comparable performance, yet the efficiency of SchNet is much better. Combining these two points, we adopt SchNet in current version of GraphMVP.

B.3 SUMMARY

To sum up, in GraphMVP, the most important message we want to deliver is how to design a well-motivated SSL algorithm to extract useful 3D geometry information to augment the 2D representation for downstream fine-tuning. GraphMVP is model-agnostic, and we may as well leave the more advanced 3D [23, 45, 58, 78] and 2D [13, 54, 102] GNN for future exploration.

In addition, molecular property prediction tasks have rich alternative representation methods, including SMILES [39, 95], and biological knowledge graph [56, 94]. There have been another SSL research line on them [21, 53, 107], yet they are beyond the scope of discussion in this paper.

C MAXIMIZE MUTUAL INFORMATION

In what follows, we will use X and Y to denote the data space for 2D graph and 3D graph respectively. Then the latent representations are denoted as h_x and h_y .

C.1 FORMULATION

The standard formulation for mutual information (MI) is

$$I(X; Y) = \mathbb{E}_{p(\mathbf{x}, \mathbf{y})} \left[\log \frac{p(\mathbf{x}, \mathbf{y})}{p(\mathbf{x})p(\mathbf{y})} \right]. \quad (17)$$

Another well-explained MI inspired from wikipedia is given in Figure 3.

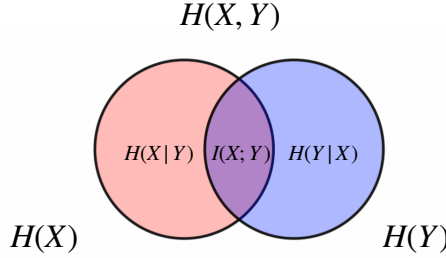


Figure 3: Venn diagram of mutual information. Inspired by wikipedia.

Mutual information (MI) between random variables measures the corresponding non-linear dependence. As can be seen in the first equation in Equation (17), the larger the divergence between the joint ($p(\mathbf{x}, \mathbf{y})$) and the product of the marginals $p(\mathbf{x})p(\mathbf{y})$, the stronger the dependence between X and Y .

Thus, following this logic, maximizing MI between 2D and 3D views can force the 3D/2D representation to capture higher-level factors, *e.g.*, the occurrence of important substructure that is semantically vital for downstream tasks. Or equivalently, maximizing MI can decrease the uncertainty in 2D representation given 3D geometric information.

C.2 A LOWER BOUND TO MI

To solve MI, we first extract a lower bound:

$$\begin{aligned} I(X; Y) &= \mathbb{E}_{p(\mathbf{x}, \mathbf{y})} \left[\log \frac{p(\mathbf{x}, \mathbf{y})}{p(\mathbf{x})p(\mathbf{y})} \right] \\ &\geq \mathbb{E}_{p(\mathbf{x}, \mathbf{y})} \left[\log \frac{p(\mathbf{x}, \mathbf{y})}{\sqrt{p(\mathbf{x})p(\mathbf{y})}} \right] \\ &= \frac{1}{2} \mathbb{E}_{p(\mathbf{x}, \mathbf{y})} \left[\log \frac{(p(\mathbf{x}, \mathbf{y}))^2}{p(\mathbf{x})p(\mathbf{y})} \right] \\ &= \frac{1}{2} \mathbb{E}_{p(\mathbf{x}, \mathbf{y})} \left[\log p(\mathbf{x}|\mathbf{y}) \right] + \frac{1}{2} \mathbb{E}_{p(\mathbf{x}, \mathbf{y})} \left[\log p(\mathbf{y}|\mathbf{x}) \right] \\ &= -\frac{1}{2}[H(Y|X) + H(X|Y)]. \end{aligned} \quad (18)$$

Thus, we transform the MI maximization problem into minimizing the following objective:

$$\mathcal{L}_{\text{MI}} = \frac{1}{2}[H(Y|X) + H(X|Y)]. \quad (19)$$

In the following sections, we will describe two self-supervised learning methods for solving MI. Notice that the methods are very general, and can be applied to various applications. Here we apply it mainly for making 3D geometry useful for 2D representation learning on molecules.

D CONTRASTIVE SELF-SUPERVISED LEARNING

The essence of contrastive self-supervised learning is to align positive view pairs and contrast negative view pairs, such that the obtained representation space is well distributed [93]. We display the pipeline in Figure 4. Along the research line in graph SSL [57, 59, 97, 99], InfoNCE and EBM-NCE are the two most-widely used, as discussed below.

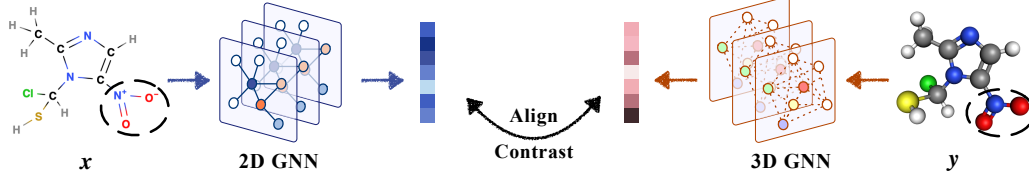


Figure 4: Contrastive SSL in GraphMVP. The black dashed circles represent subgraph masking.

D.1 INFONCE

InfoNCE [69] is first proposed to approximate MI Equation (17):

$$\mathcal{L}_{\text{InfoNCE}} = -\frac{1}{2} \mathbb{E} \left[\log \frac{\exp(f_{\mathbf{x}}(\mathbf{x}, \mathbf{y}))}{\exp(f_{\mathbf{x}}(\mathbf{x}, \mathbf{y})) + \sum_j \exp(f_{\mathbf{x}}(\mathbf{x}^j, \mathbf{y}))} + \log \frac{\exp(f_{\mathbf{y}}(\mathbf{y}, \mathbf{x}))}{\exp(f_{\mathbf{y}}(\mathbf{y}, \mathbf{x})) + \sum_j \exp(f_{\mathbf{y}}(\mathbf{y}^j, \mathbf{x}))} \right], \quad (20)$$

where $\mathbf{x}^j, \mathbf{y}^j$ are randomly sampled 2D and 3D views regarding to the anchored pair (\mathbf{x}, \mathbf{y}) . $f_{\mathbf{x}}(\mathbf{x}, \mathbf{y}), f_{\mathbf{y}}(\mathbf{y}, \mathbf{x})$ are scoring functions for the two corresponding views, whose formulation can be quite flexible. Here we use $f_{\mathbf{x}}(\mathbf{x}, \mathbf{y}) = f_{\mathbf{y}}(\mathbf{y}, \mathbf{x}) = \exp(\langle h_{\mathbf{x}}, h_{\mathbf{y}} \rangle)$.

Derivation of InfoNCE

$$\begin{aligned} I(X; Y) - \log(K) &= \mathbb{E}_{p(\mathbf{x}, \mathbf{y})} \left[\log \frac{1}{K} \frac{p(\mathbf{x}, \mathbf{y})}{p(\mathbf{x})p(\mathbf{y})} \right] \\ &= \sum_{\mathbf{x}^i, \mathbf{y}^i} \left[\log \frac{1}{K} \frac{p(\mathbf{x}^i, \mathbf{y}^i)}{p(\mathbf{x}^i)p(\mathbf{y}^i)} \right] \\ &\geq - \sum_{\mathbf{x}^i, \mathbf{y}^i} \left[\log \left(1 + (K-1) \frac{p(\mathbf{x}^i)p(\mathbf{y}^i)}{p(\mathbf{x}^i)p(\mathbf{y}^i)} \right) \right] \\ &= - \sum_{\mathbf{x}^i, \mathbf{y}^i} \left[\log \frac{\frac{p(\mathbf{x}^i, \mathbf{y}^i)}{p(\mathbf{x}^i)p(\mathbf{y}^i)} + (K-1)}{\frac{p(\mathbf{x}^i, \mathbf{y}^i)}{p(\mathbf{x}^i)p(\mathbf{y}^i)}} \right] \\ &\approx - \sum_{\mathbf{x}^i, \mathbf{y}^i} \left[\log \frac{\frac{p(\mathbf{x}^i, \mathbf{y}^i)}{p(\mathbf{x}^i)p(\mathbf{y}^i)} + (K-1)\mathbb{E}_{\mathbf{x}^j \neq \mathbf{x}^i} \frac{p(\mathbf{x}^j, \mathbf{y}^i)}{p(\mathbf{x}^j)p(\mathbf{y}^i)}}{\frac{p(\mathbf{x}^i, \mathbf{y}^i)}{p(\mathbf{x}^i)p(\mathbf{y}^i)}} \right] \quad // \textcircled{1} \\ &= \sum_{\mathbf{x}^i, \mathbf{y}^i} \left[\log \frac{\exp(f_{\mathbf{x}}(\mathbf{x}^i, \mathbf{y}^i))}{\exp(f_{\mathbf{x}}(\mathbf{x}^i, \mathbf{y}^i)) + \sum_{j=1}^K \exp(f_{\mathbf{x}}(\mathbf{x}^j, \mathbf{y}^i))} \right], \end{aligned} \quad (21)$$

where we set $f_{\mathbf{x}}(\mathbf{x}^i, \mathbf{y}^i) = \log \frac{p(\mathbf{x}^i, \mathbf{y}^i)}{p(\mathbf{x}^i)p(\mathbf{y}^i)}$.

Notice that in $\textcircled{1}$, we are using data $x \in X$ as the anchor points. If we use the $y \in Y$ as the anchor points and follow the similar steps, we can obtain

$$I(X; Y) - \log(K) \geq \sum_{\mathbf{y}^i, \mathbf{x}^i} \left[\log \frac{\exp(f_{\mathbf{y}}(\mathbf{y}^i, \mathbf{x}^i))}{\exp(f_{\mathbf{y}}(\mathbf{y}^i, \mathbf{x}^i)) + \sum_{j=1}^K \exp(f_{\mathbf{y}}(\mathbf{y}^j, \mathbf{x}^i))} \right]. \quad (22)$$

Thus, by add both together, we can have the objective function as Equation (20).

D.2 EBM-NCE

We here provide an alternative approach to maximizing MI using energy-based model (EBM). To our best knowledge, we are the **first** to give the rigorous proof of using EBM to maximize the MI.

D.2.1 ENERGY-BASED MODEL (EBM)

Energy-based model (EBM) is a powerful tool for modeling the data distribution. The classic formulation is:

$$p(\mathbf{x}) = \frac{\exp(-E(\mathbf{x}))}{A}, \quad (23)$$

where the bottleneck is the intractable partition function $A = \int_{\mathbf{x}} \exp(-E(\mathbf{x}))d\mathbf{x}$. Recently, there have been quite a lot progress along this direction [19, 32, 80, 81]. Noise Contrastive Estimation (NCE) [32] is one of the powerful tools here, as we will introduce later.

D.2.2 EBM FOR MI

Recall that our objective function is Equation (19): $\mathcal{L}_{\text{MI}} = \frac{1}{2}[H(Y|X) + H(X|Y)]$. Then we model the conditional likelihood with energy-based model (EBM). This gives us

$$\mathcal{L}_{\text{EBM}} = -\frac{1}{2}\mathbb{E}_{p(\mathbf{x}, \mathbf{y})} \left[\log \frac{\exp(f_{\mathbf{x}}(\mathbf{x}, \mathbf{y}))}{A_{\mathbf{x}|\mathbf{y}}} + \log \frac{\exp(f_{\mathbf{y}}(\mathbf{y}, \mathbf{x}))}{A_{\mathbf{y}|\mathbf{x}}} \right], \quad (24)$$

where $f_{\mathbf{x}}(\mathbf{x}, \mathbf{y}) = -E(\mathbf{x}|\mathbf{y})$ and $f_{\mathbf{y}}(\mathbf{y}, \mathbf{x}) = -E(\mathbf{y}|\mathbf{x})$ are the negative energy functions, and $A_{\mathbf{x}|\mathbf{y}}$ and $A_{\mathbf{y}|\mathbf{x}}$ are the corresponding partition functions.

Under the EBM framework, if we solve Equation (24) with Noise Contrastive Estimation (NCE) [32], the final EBM-NCE objective is

$$\begin{aligned} \mathcal{L}_{\text{EBM-NCE}} &= -\frac{1}{2}\mathbb{E}_{p_{\text{data}}(\mathbf{y})} \left[\mathbb{E}_{p_n(\mathbf{x}|\mathbf{y})} [\log(1 - \sigma(f_{\mathbf{x}}(\mathbf{x}, \mathbf{y})))] + \mathbb{E}_{p_{\text{data}}(\mathbf{x}|\mathbf{y})} [\log \sigma(f_{\mathbf{x}}(\mathbf{x}, \mathbf{y}))] \right] \\ &\quad - \frac{1}{2}\mathbb{E}_{p_{\text{data}}(\mathbf{x})} \left[\mathbb{E}_{p_n(\mathbf{y}|\mathbf{x})} [\log(1 - \sigma(f_{\mathbf{y}}(\mathbf{y}, \mathbf{x})))] + \mathbb{E}_{p_{\text{data}}(\mathbf{y}|\mathbf{x})} [\log \sigma(f_{\mathbf{y}}(\mathbf{y}, \mathbf{x}))] \right]. \end{aligned} \quad (25)$$

Next we will give the detailed derivations.

D.2.3 DERIVATION OF CONDITIONAL EBM WITH NCE

WLOG, let's consider the $p_{\theta}(\mathbf{x}|\mathbf{y})$ first, and by EBM it is as follows:

$$p_{\theta}(\mathbf{x}|\mathbf{y}) = \frac{\exp(-E(\mathbf{x}|\mathbf{y}))}{\int \exp(-E(\tilde{\mathbf{x}}|\mathbf{y}))d\tilde{\mathbf{x}}} = \frac{\exp(f_{\mathbf{x}}(\mathbf{x}, \mathbf{y}))}{\int \exp(f_{\mathbf{x}}(\tilde{\mathbf{x}}|\mathbf{y}))d\tilde{\mathbf{x}}} = \frac{\exp(f_{\mathbf{x}}(\mathbf{x}, \mathbf{y}))}{A_{\mathbf{x}|\mathbf{y}}}. \quad (26)$$

Then we solve this using NCE. NCE handles the intractability issue by transforming it as a binary classification task. We take the partition function $A_{\mathbf{x}|\mathbf{y}}$ as a parameter, and introduce a noise distribution p_n . Based on this, we introduce a mixture model: $z = 0$ if the conditional $\mathbf{x}|\mathbf{y}$ is from $p_n(\mathbf{x}|\mathbf{y})$, and $z = 1$ if $\mathbf{x}|\mathbf{y}$ is from $p_{\text{data}}(\mathbf{x}|\mathbf{y})$. So the joint distribution is:

$$p_{n,\text{data}}(\mathbf{x}|\mathbf{y}) = p(z=1)p_{\text{data}}(\mathbf{x}|\mathbf{y}) + p(z=0)p_n(\mathbf{x}|\mathbf{y})$$

The posterior of $p(z=0|\mathbf{x}, \mathbf{y})$ is

$$p_{n,\text{data}}(z=0|\mathbf{x}, \mathbf{y}) = \frac{p(z=0)p_n(\mathbf{x}|\mathbf{y})}{p(z=0)p_n(\mathbf{x}|\mathbf{y}) + p(z=1)p_{\text{data}}(\mathbf{x}|\mathbf{y})} = \frac{\nu \cdot p_n(\mathbf{x}|\mathbf{y})}{\nu \cdot p_n(\mathbf{x}|\mathbf{y}) + p_{\text{data}}(\mathbf{x}|\mathbf{y})},$$

where $\nu = \frac{p(z=0)}{p(z=1)}$.

Similarly, we can have the joint distribution under EBM framework as:

$$p_{n,\theta}(\mathbf{x}) = p(z=0)p_n(\mathbf{x}|\mathbf{y}) + p(z=1)p_{\theta}(\mathbf{x}|\mathbf{y})$$

And the corresponding posterior is:

$$p_{n,\theta}(z=0|\mathbf{x}, \mathbf{y}) = \frac{p(z=0)p_n(\mathbf{x}|\mathbf{y})}{p(z=0)p_n(\mathbf{x}|\mathbf{y}) + p(z=1)p_{\theta}(\mathbf{x}|\mathbf{y})} = \frac{\nu \cdot p_n(\mathbf{x}|\mathbf{y})}{\nu \cdot p_n(\mathbf{x}|\mathbf{y}) + p_{\theta}(\mathbf{x}|\mathbf{y})}$$

We indirectly match $p_\theta(\mathbf{x}|\mathbf{y})$ to $p_{\text{data}}(\mathbf{x}|\mathbf{y})$ by fitting $p_{n,\theta}(\mathbf{z}|\mathbf{x}, \mathbf{y})$ to $p_{n,\text{data}}(\mathbf{z}|\mathbf{x}, \mathbf{y})$ by minimizing their KL-divergence:

$$\begin{aligned}
& \min_{\theta} D_{\text{KL}}(p_{n,\text{data}}(\mathbf{z}|\mathbf{x}, \mathbf{y}) || p_{n,\theta}(\mathbf{z}|\mathbf{x}, \mathbf{y})) \\
&= \mathbb{E}_{p_{n,\text{data}}(\mathbf{x}, \mathbf{z}|\mathbf{y})} [\log p_{n,\theta}(\mathbf{z}|\mathbf{x}, \mathbf{y})] \\
&= \int \sum_{\mathbf{z}} p_{n,\text{data}}(\mathbf{x}, \mathbf{z}|\mathbf{y}) \cdot \log p_{n,\theta}(\mathbf{z}|\mathbf{x}, \mathbf{y}) d\mathbf{x} \\
&= \int \left\{ p(\mathbf{z}=0)p_{n,\text{data}}(\mathbf{x}|\mathbf{y}, \mathbf{z}=0) \log p_{n,\theta}(\mathbf{z}=0|\mathbf{x}, \mathbf{y}) \right. \\
&\quad \left. + p(\mathbf{z}=1)p_{n,\text{data}}(\mathbf{x}|\mathbf{z}=1, \mathbf{y}) \log p_{n,\theta}(\mathbf{z}=1|\mathbf{x}, \mathbf{y}) \right\} d\mathbf{x} \\
&= \nu \cdot \mathbb{E}_{p_n(\mathbf{x}|\mathbf{y})} \left[\log p_{n,\theta}(\mathbf{z}=0|\mathbf{x}, \mathbf{y}) \right] + \mathbb{E}_{p_{\text{data}}(\mathbf{x}|\mathbf{y})} \left[\log p_{n,\theta}(\mathbf{z}=1|\mathbf{x}, \mathbf{y}) \right] \\
&= \nu \cdot \mathbb{E}_{p_n(\mathbf{x}|\mathbf{y})} \left[\log \frac{\nu \cdot p_n(\mathbf{x}|\mathbf{y})}{\nu \cdot p_n(\mathbf{x}|\mathbf{y}) + p_\theta(\mathbf{x}|\mathbf{y})} \right] + \mathbb{E}_{p_{\text{data}}(\mathbf{x}|\mathbf{y})} \left[\log \frac{p_\theta(\mathbf{x}|\mathbf{y})}{\nu \cdot p_n(\mathbf{x}|\mathbf{y}) + p_\theta(\mathbf{x}|\mathbf{y})} \right]. \tag{27}
\end{aligned}$$

This optimal distribution is an estimation to the actual distribution (or data distribution), *i.e.*, $p_\theta(\mathbf{x}|\mathbf{y}) \approx p_{\text{data}}(\mathbf{x}|\mathbf{y})$. We can follow the similar steps for $p_\theta(\mathbf{y}|\mathbf{x}) \approx p_{\text{data}}(\mathbf{y}|\mathbf{x})$. Thus following Equation (27), the objective function is to maximize

$$\nu \cdot \mathbb{E}_{p_{\text{data}}(\mathbf{y})} \mathbb{E}_{p_n(\mathbf{x}|\mathbf{y})} \left[\log \frac{\nu \cdot p_n(\mathbf{x}|\mathbf{y})}{\nu \cdot p_n(\mathbf{x}|\mathbf{y}) + p_\theta(\mathbf{x}|\mathbf{y})} \right] + \mathbb{E}_{p_{\text{data}}(\mathbf{y})} \mathbb{E}_{p_{\text{data}}(\mathbf{x}|\mathbf{y})} \left[\log \frac{p_\theta(\mathbf{x}|\mathbf{y})}{\nu \cdot p_n(\mathbf{x}|\mathbf{y}) + p_\theta(\mathbf{x}|\mathbf{y})} \right]. \tag{28}$$

The we will adopt three strategies to approximate Equation (28):

- Self-normalization.** When the EBM is very expressive, *i.e.*, using deep neural network for modeling, we can assume it is able to approximate the normalized density directly [64, 80]. In other words, we can set the partition function $A = 1$. This is a self-normalized EBM-NCE, with normalizing constant close to 1, *i.e.*, $p(\mathbf{x}) = \exp(-E(\mathbf{x})) = \exp(f(\mathbf{x}))$ in Equation (23).
- Exponential tilting term.** Exponential tilting term [2] is another useful trick. It models the distribution as $\tilde{p}_\theta(\mathbf{x}) = q(\mathbf{x}) \exp(-E_\theta(\mathbf{x}))$, where $q(\mathbf{x})$ is the reference distribution. If we use the same reference distribution as the noise distribution, the tilted probability is $\tilde{p}_\theta(\mathbf{x}) = p_n(\mathbf{x}) \exp(-E_\theta(\mathbf{x}))$ in Equation (23).
- Sampling.** For many cases, we only need to sample 1 negative points for each data, *i.e.*, $\nu = 1$.

Following these three disciplines, the objective function to optimize $p_\theta(\mathbf{x}|\mathbf{y})$ becomes

$$\begin{aligned}
& \mathbb{E}_{p_n(\mathbf{x}|\mathbf{y})} \left[\log \frac{p_n(\mathbf{x}|\mathbf{y})}{p_n(\mathbf{x}|\mathbf{y}) + \tilde{p}_\theta(\mathbf{x}|\mathbf{y})} \right] + \mathbb{E}_{p_{\text{data}}(\mathbf{x}|\mathbf{y})} \left[\log \frac{\tilde{p}_\theta(\mathbf{x}|\mathbf{y})}{p_n(\mathbf{x}|\mathbf{y}) + \tilde{p}_\theta(\mathbf{x}|\mathbf{y})} \right] \\
&= \mathbb{E}_{p_n(\mathbf{x}|\mathbf{y})} \left[\log \frac{1}{1 + p_\theta(\mathbf{x}|\mathbf{y})} \right] + \mathbb{E}_{p_{\text{data}}(\mathbf{x}|\mathbf{y})} \left[\log \frac{p_\theta(\mathbf{x}|\mathbf{y})}{1 + p_\theta(\mathbf{x}|\mathbf{y})} \right] \\
&= \mathbb{E}_{p_n(\mathbf{x}|\mathbf{y})} \left[\log \frac{\exp(-f_\mathbf{x}(\mathbf{x}, \mathbf{y}))}{\exp(-f_\mathbf{x}(\mathbf{x}, \mathbf{y})) + 1} \right] + \mathbb{E}_{p_{\text{data}}(\mathbf{x}|\mathbf{y})} \left[\log \frac{1}{\exp(-f_\mathbf{x}(\mathbf{x}, \mathbf{y})) + 1} \right] \\
&= \mathbb{E}_{p_n(\mathbf{x}|\mathbf{y})} \left[\log (1 - \sigma(f_\mathbf{x}(\mathbf{x}, \mathbf{y}))) \right] + \mathbb{E}_{p_{\text{data}}(\mathbf{x}|\mathbf{y})} \left[\log \sigma(f_\mathbf{x}(\mathbf{x}, \mathbf{y})) \right]. \tag{29}
\end{aligned}$$

Thus, the final EBM-NCE contrastive SSL objective is

$$\begin{aligned}
\mathcal{L}_{\text{EBM-NCE}} &= -\frac{1}{2} \mathbb{E}_{p_{\text{data}}(\mathbf{y})} \left[\mathbb{E}_{p_n(\mathbf{x}|\mathbf{y})} \log (1 - \sigma(f_\mathbf{x}(\mathbf{x}, \mathbf{y}))) + \mathbb{E}_{p_{\text{data}}(\mathbf{x}|\mathbf{y})} \log \sigma(f_\mathbf{x}(\mathbf{x}, \mathbf{y})) \right] \\
&\quad - \frac{1}{2} \mathbb{E}_{p_{\text{data}}(\mathbf{x})} \left[\mathbb{E}_{p_n(\mathbf{y}|\mathbf{x})} \log (1 - \sigma(f_\mathbf{y}(\mathbf{y}, \mathbf{x}))) + \mathbb{E}_{p_{\text{data}}(\mathbf{y}, \mathbf{x})} \log \sigma(f_\mathbf{y}(\mathbf{y}, \mathbf{x})) \right]. \tag{30}
\end{aligned}$$

D.3 EBM-NCE v.s. JSE AND INFONCE

We acknowledge that there are many other contrastive objectives [73] that can be used to maximize MI. However, in the research line of graph SSL, as summarized in several recent survey papers [59, 97, 99], the two most used ones are InfoNCE and Jensen-Shannon Estimator (JSE) [40, 68].

We conclude that JSE is very similar to EBM-NCE, while the underlying perspectives are totally different, as explained below.

1. **Derivation and Intuition.** Derivation process and underlying intuition are different. JSE [68] starts from f-divergence, then with variational estimation and Fenchel duality on function f . Our proposed EBM-NCE is more straightforward: it models the conditional distribution in the MI lower bound Equation (19) with EBM, and solves it using NCE.
2. **Flexibility.** Modeling the conditional distribution with EBM provides a broader family of algorithms. NCE is just one solution to it, and recent progress on score matching [80, 81] and contrastive divergence [19], though no longer contrastive SSL, adds on more promising directions. Thus, EBM can provide a potential unified framework for structuring our understanding of self-supervised learning.
3. **Noise distribution.** Starting from [40], all the following works on graph SSL [59, 82, 97, 99] have been adopting the empirical distribution for noise distribution. However, this is not the case in EBM-NCE. Classic EBM-NCE uses fixed distribution, while more recent work [2] extends it with adaptively learnable noise distribution. With this discipline, more advanced sampling strategies (w.r.t. the noise distribution) can be proposed, *e.g.*, adversarial negative sampling in [41].

In the above, we conclude three key differences between EBM-NCE and JSE, plus the solid and straightforward derivations on EBM-NCE. We believe this can provide a insightful perspective of SSL to the community.

According to the empirical results Section 4.4, we observe that EBM-NCE is better than InfoNCE. This can be explained using the claim from [47], where the main technical contribution is to construct many positives and many negatives per anchor point. The binary cross-entropy in EBM-NCE is able to realize this to some extent: make all the positive pairs positive and all the negative pairs negative, where the softmax-based cross-entropy fails to capture this, as in InfoNCE.

To conclude, we are introduce using EBM in modeling MI, which opens many potential venues. As for contrastive SSL, EBM-NCE provides a better perspective than JSE, and is better than InfoNCE on graph-level self-supervised learning.

E GENERATIVE SELF-SUPERVISED LEARNING

Generative SSL is another classic track for unsupervised pre-training [48, 49, 51], though the main focus is on distribution learning. In GraphMVP, we start with VAE for the following reasons:

1. One of the biggest attributes of our problem is that the mapping between two views are stochastic: multiple 3D conformers can correspond to the same 2D topology. Thus, we expect a stochastic model [67] like VAE, instead of the deterministic ones.
2. For pre-training and fine-tuning, we need to learn an explicit and powerful representation function that can be used for downstream tasks.
3. The decoder for structured data like graph are often complicated, *e.g.*, the auto-regressive generation. This makes them suboptimal.

To cope with these challenges, in GraphMVP, we start with VAE-like generation model, and later propose a *light-weighted* and *smart* surrogate loss as objective function. Notice that for notation simplicity, for this section, we use h_y and h_x to delegate the 2D and 3D GNN respectively.

E.1 VARIATIONAL MOLECULE RECONSTRUCTION

As shown in Equation (19), our main motivation is to model the conditional likelihood:

$$\mathcal{L}_{\text{MI}} = -\frac{1}{2} \mathbb{E}_{p(\mathbf{x}, \mathbf{y})} [\log p(\mathbf{x}|\mathbf{y}) + \log p(\mathbf{y}|\mathbf{x})]$$

By introducing a reparameterized variable $\mathbf{z}_x = \mu_x + \sigma_x \odot \epsilon$, where μ_x and σ_x are two flexible functions on h_x , $\epsilon \sim \mathcal{N}(0, I)$ and \odot is the element-wise production, we have a lower bound on the conditional likelihood:

$$\log p(\mathbf{y}|\mathbf{x}) \geq \mathbb{E}_{q(\mathbf{z}_x|\mathbf{x})} [\log p(\mathbf{y}|\mathbf{z}_x)] - KL(q(\mathbf{z}_x|\mathbf{x})||p(\mathbf{z}_x)). \quad (31)$$

Similarly, we have

$$\log p(\mathbf{x}|\mathbf{y}) \geq \mathbb{E}_{q(\mathbf{z}_y|\mathbf{y})} [\log p(\mathbf{x}|\mathbf{z}_y)] - KL(q(\mathbf{z}_y|\mathbf{y})||p(\mathbf{z}_y)), \quad (32)$$

where $\mathbf{z}_y = \mu_y + \sigma_y \odot \epsilon$. Here μ_y and σ_y are flexible functions on h_y , and $\epsilon \sim \mathcal{N}(0, I)$. For implementation, we take multi-layer perceptrons (MLPs) for $\mu_x, \mu_y, \sigma_x, \sigma_y$.

Both the above objectives are composed of a conditional log-likelihood and a KL-divergence. The conditional log-likelihood has also been recognized as the *reconstruction term*: it is essentially to reconstruct the 3D conformers (\mathbf{y}) from the sampled 2D molecular graph representation (\mathbf{z}_x). However, performing the graph reconstruction on the data space is not easy: since molecules are discrete, modeling and measuring are not trivial.

E.2 VARIATIONAL REPRESENTATION RECONSTRUCTION

To cope with data reconstruction issue, we propose a novel generative loss termed variation representation reconstruction (VRR). The pipeline is in Figure 5.

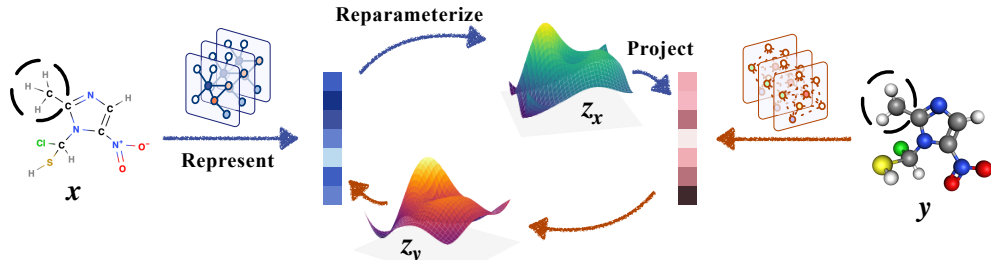


Figure 5: VRR SSL in GraphMVP. The black dashed circles represent subgraph masking.

Our proposed solution is very straightforward. Recall that MI is invariant to continuous bijective function [7]. So suppose we have a representation function h_y satisfying this condition, and this can guide us a surrogate loss by transferring the reconstruction from data space to the continuous representation space:

$$\mathbb{E}_{q(\mathbf{z}_x|\mathbf{x})}[\log p(\mathbf{y}|\mathbf{z}_x)] = -\mathbb{E}_{q(\mathbf{z}_x|\mathbf{x})}[\|h_y(g_x(\mathbf{z}_x)) - h_y(\mathbf{y})\|_2^2] + C,$$

where g_x is the decoder and C is a constant, and this introduces to using the mean-squared error (MSE) for **reconstruction on the representation space**.

Then for the reconstruction, current formula has two steps: i) the latent code \mathbf{z}_x is first mapped to molecule space, and ii) it is mapped to the representation space. We can approximate these two mappings with one projection step, by directly projecting the latent code \mathbf{z}_x to the 3D representation space, *i.e.*, $q_x(\mathbf{z}_x) \approx h_y(g_x(\mathbf{z}_x))$. This gives us a variation representation reconstruction (VRR) SSL objective as below:

$$\mathbb{E}_{q(\mathbf{z}_x|\mathbf{x})}[\log p(\mathbf{y}|\mathbf{z}_x)] = -\mathbb{E}_{q(\mathbf{z}_x|\mathbf{x})}[\|q_x(\mathbf{z}_x) - h_y(\mathbf{y})\|_2^2] + C.$$

β -VAE We consider introducing a β variable [38] to control the disentanglement of the latent representation. To be more specific, we would have

$$\log p(\mathbf{y}|\mathbf{x}) \geq \mathbb{E}_{q(\mathbf{z}_x|\mathbf{x})}[\log p(\mathbf{y}|\mathbf{z}_x)] - \beta \cdot KL(q(\mathbf{z}_x|\mathbf{x})||p(\mathbf{z}_x)). \quad (33)$$

Stop-gradient For the optimization on variational representation reconstruction, related work have found that adding the stop-gradient operator (SG) as a regularizer can make the training more stable without collapse both empirically [12, 31] and theoretically [84]. Here, we may as well utilize this SG operation in the objective function:

$$\mathbb{E}_{q(\mathbf{z}_x|\mathbf{x})}[\log p(\mathbf{y}|\mathbf{z}_x)] = -\mathbb{E}_{q(\mathbf{z}_x|\mathbf{x})}[\|q_x(\mathbf{z}_x) - SG(h_y(\mathbf{y}))\|_2^2] + C. \quad (34)$$

Objective function for VRR Thus, combining both two regularizers mentioned above, the final objective function for VRR is:

$$\begin{aligned} \mathcal{L}_{\text{VRR}} &= \frac{1}{2} \left[\mathbb{E}_{q(\mathbf{z}_x|\mathbf{x})}[\|q_x(\mathbf{z}_x) - SG(h_y(\mathbf{y}))\|_2^2] + \mathbb{E}_{q(\mathbf{z}_y|\mathbf{y})}[\|q_y(\mathbf{z}_y) - SG(h_x(\mathbf{y}))\|_2^2] \right] \\ &\quad + \frac{\beta}{2} \cdot \left[KL(q(\mathbf{z}_x|\mathbf{x})||p(\mathbf{z}_x)) + KL(q(\mathbf{z}_y|\mathbf{y})||p(\mathbf{z}_y)) \right]. \end{aligned} \quad (35)$$

Note that MI is invariant to continuous bijective function [7], thus this surrogate loss would be exact if the encoding function h_y and h_x satisfy this condition. However, we find GNN (both GIN and SchNet) can, though do not meet the condition, provide quite robust performance empirically, which justify the effectiveness of VRR.

E.3 VARIATIONAL REPRESENTATION RECONSTRUCTION AND NON-CONTRASTIVE SSL

By introducing VRR, we provide another perspective to understand the generative SSL, including the recently-proposed non-contrastive SSL [12, 31].

We provide a unified structure on the intra-data generative SSL:

- Reconstruction to the data space, like Equations (5), (31) and (32).
- Reconstruction to the representation space, *i.e.*, VRR in Equation (35).
 - If we **remove the stochasticity**, then it is simply the representation reconstruction (RR), as we tested in the ablation study Section 4.4.
 - If we **remove the stochasticity** and assume two views are **sharing the same representation function**, like CNN for multi-view learning on images, then it is reduced to the BYOL [31] and SimSiam [12]. In other words, these recently-proposed non-contrastive SSL methods are indeed special cases of VRR.

F DATASET OVERVIEW

F.1 PRE-TRAINING DATASET OVERVIEW

In this section, we provide the basic statistics of the pre-training dataset (GEOM).

In Figure 6, we plot the histogram (logarithm scale on the y-axis) and cumulative distribution on the number of conformers of each molecule. As shown by the histogram and curves, there are certain number of molecules having over 1000 possible 3d conformer structures, while over 80% of molecules have less than 100 conformers.

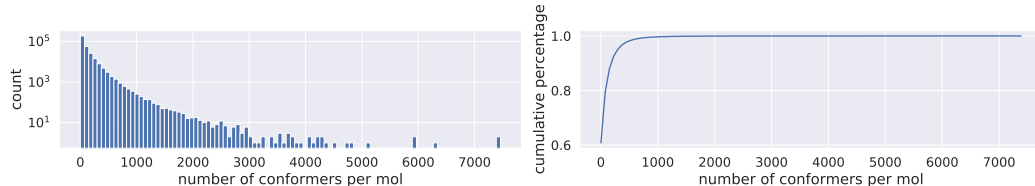


Figure 6: Statistics on the conformers of each molecule

In Figure 6, we plot the histogram of the summation of top (descending sorted by weights) {1,5,10,20} conformer weights. The physical meaning of the weight is the portion of each conformer occurred in nature. We observe that the top 5 or 10 conformers are sufficient as they have dominated nearly all the natural observations. Such long-tailed distribution is also in alignment with our findings in the ablation studies. We find that utilizing top five conformers in the GraphMVP has reached an idealised spot between effectiveness and efficiency.

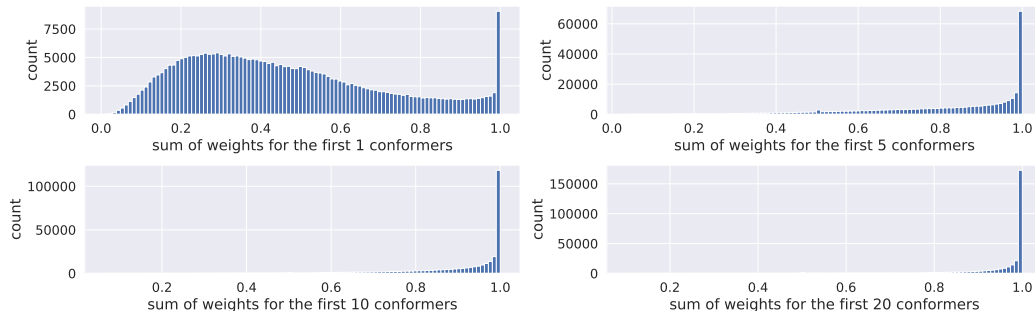


Figure 7: Sum of occurrence weights for the top major conformers

F.2 DOWNSTREAM DATASET OVERVIEW

In this section, we review the four main categories of datasets used for downstream tasks.

Molecular Property: Pharmacology The Blood-Brain Barrier Penetration (BBBP) [61] dataset measures whether a molecule will penetrate the central nervous system. All three datasets, Tox21 [85], ToxCast [98], and ClinTox [28] are related to the toxicity of molecular compounds. The Side Effect Resource (SIDER) [50] dataset stores the adverse drug reactions on a marketed drug database.

Molecular Property: Physical Chemistry Dataset proposed in [15] measures aqueous solubility of the molecular compounds. Lipophilicity (Lipo) dataset is a subset of ChEMBL [27] measuring the molecule octanol/water distribution coefficient. CEP dataset is a subset of the Harvard Clean Energy Project (CEP) [33], which estimates the organic photovoltaic efficiency.

Molecular Property: Biophysics Maximum Unbiased Validation (MUV) [76] is another sub-database from PCBA, and is obtained by applying a refined nearest neighbor analysis. HIV is from

the Drug Therapeutics Program (DTP) AIDS Antiviral Screen [105], and it aims at predicting inhibit HIV replication. BACE measures the binding results for a set of inhibitors of β -secretase 1 (BACE-1), and is gathered in MoleculeNet [98]. Malaria [24] measures the drug efficacy against the parasite that causes malaria.

Drug-Target Affinity Davis [14] measures the binding affinities between kinase inhibitors and kinases, scored by the K_d value (kinase dissociation constant). KIBA [83] contains binding affinities for kinase inhibitors from different sources, including K_i , K_d and IC_{50} . KIBA scores [70] are constructed to optimize the consistency among these values.

Table 8: Summary for the molecule chemical datasets.

Dataset	Task	# Tasks	# Molecules	# Proteins	# Molecule-Protein pairs
BBBP	Classification	1	2,039	-	-
Tox21	Classification	12	7,831	-	-
ToxCast	Classification	617	8,576	-	-
Sider	Classification	27	1,427	-	-
ClinTox	Classification	2	1,478	-	-
MUV	Classification	17	93,087	-	-
HIV	Classification	1	41,127	-	-
Bace	Classification	1	1,513	-	-
Delaney	Regression	1	1,128	-	-
Lipo	Regression	1	4,200	-	-
Malaria	Regression	1	9,999	-	-
CEP	Regression	1	29,978	-	-
Davis	Regression	1	68	379	30,056
KIBA	Regression	1	2,068	229	118,254

G EXPERIMENTS DETAILS

G.1 SELF-SUPERVISED LEARNING BASELINES

For the SSL baselines in main results (Table 1), generally we can match with the original paper, even though most of them are using larger pre-training datasets, like ZINC-2m. Yet, we would like to add some specifications.

- G-{Contextual, Motif}[77] proposes a new GNN model for backbone model, and does pre-training on a larger dataset. Both settings are different from us.
- JOAO [103] has two versions in the original paper. In this paper, we run both versions and report the optimal one.
- Almost all the graph SSL baselines are reporting the test performance with optimal validation error, while GraphLoG [101] reports 73.2 in the paper with the last-epoch performance. This can be over-optimized in terms of overfitting, and here we rerun it with the same downstream evaluation strategy as a fair comparison.

G.2 ABLATION STUDY: THE EFFECT OF MASKING RATIO AND NUMBER OF CONFORMERS

Table 9: Full results for ablation of masking ratio M ($C = 0.15$), MVP is short for GraphMVP.

	M	BBBP	Tox21	ToxCast	Sider	ClinTox	MUV	HIV	Bace	Avg
-	-	65.4(2.4)	74.9(0.8)	61.6(1.2)	58.0(2.4)	58.8(5.5)	71.0(2.5)	75.3(0.5)	72.6(4.9)	67.21
MVP	0	69.4 (1.0)	75.3 (0.5)	62.8 (0.2)	61.9 (0.5)	74.4 (1.3)	74.6 (1.4)	74.6 (1.0)	76.0 (2.0)	71.12
	0.15	68.5 (0.2)	74.5 (0.4)	62.7 (0.1)	62.3 (1.6)	79.0 (2.5)	75.0 (1.4)	74.8 (1.4)	76.8 (1.1)	71.69
	0.3	68.6 (0.3)	74.9 (0.6)	62.8 (0.4)	60.0 (0.6)	74.8 (7.8)	74.7 (0.8)	75.5 (1.1)	82.9 (1.7)	71.79
MVP-G	0	72.4 (1.3)	74.7 (0.6)	62.4 (0.2)	60.3 (0.7)	76.2 (5.7)	76.6 (1.7)	76.4 (1.7)	78.0 (1.1)	72.15
	0.15	70.8 (0.5)	75.9 (0.5)	63.1 (0.2)	60.2 (1.1)	79.1 (2.8)	77.7 (0.6)	76.0 (0.1)	79.3 (1.5)	72.76
	0.3	69.5 (0.5)	74.6 (0.6)	62.7 (0.3)	60.8 (1.2)	80.7 (2.0)	77.8 (2.5)	76.2 (0.5)	81.0 (1.0)	72.91
MVP-C	0	71.5 (0.9)	75.4 (0.3)	63.6 (0.5)	61.8 (0.6)	77.3 (1.2)	75.8 (0.6)	76.1 (0.9)	79.8 (0.4)	72.66
	0.15	72.4 (1.6)	74.4 (0.2)	63.1 (0.4)	63.9 (1.2)	77.5 (4.2)	75.0 (1.0)	77.0 (1.2)	81.2 (0.9)	73.07
	0.3	70.7 (0.8)	74.6 (0.3)	63.8 (0.7)	60.4 (0.6)	83.5 (3.2)	74.2 (1.6)	76.0 (1.0)	82.2 (2.2)	73.17

Table 10: Full results for ablation of # conformers C ($M = 0.5$), MVP is short for GraphMVP.

	C	BBBP	Tox21	ToxCast	Sider	ClinTox	MUV	HIV	Bace	Avg
-	-	65.4(2.4)	74.9(0.8)	61.6(1.2)	58.0(2.4)	58.8(5.5)	71.0(2.5)	75.3(0.5)	72.6(4.9)	67.21
MVP	1	69.2 (1.0)	74.7 (0.4)	62.5 (0.2)	63.0 (0.4)	73.9 (7.2)	76.2 (0.4)	75.3 (1.1)	78.0 (0.5)	71.61
	5	68.5 (0.2)	74.5 (0.4)	62.7 (0.1)	62.3 (1.6)	79.0 (2.5)	75.0 (1.4)	74.8 (1.4)	76.8 (1.1)	71.69
	10	68.3 (0.5)	74.2 (0.6)	63.2 (0.5)	61.4 (1.0)	80.6 (0.8)	75.4 (2.4)	75.5 (0.6)	79.1 (2.3)	72.20
	20	68.7 (0.5)	74.9 (0.3)	62.7 (0.3)	60.8 (0.7)	75.8 (0.5)	76.3 (1.5)	77.4 (0.3)	82.3 (0.8)	72.39
MVP-G	1	70.9 (0.4)	75.3 (0.7)	62.8 (0.5)	61.2 (0.6)	81.4 (3.7)	74.2 (2.1)	76.4 (0.6)	80.2 (0.7)	72.80
	5	70.8 (0.5)	75.9 (0.5)	63.1 (0.2)	60.2 (1.1)	79.1 (2.8)	77.7 (0.6)	76.0 (0.1)	79.3 (1.5)	72.76
	10	70.2 (0.9)	74.9 (0.4)	63.4 (0.4)	60.8 (1.0)	80.6 (0.4)	76.4 (2.0)	77.0 (0.3)	77.4 (1.3)	72.59
	20	69.5 (0.4)	74.9 (0.4)	63.3 (0.1)	60.8 (0.3)	81.2 (0.5)	77.3 (2.7)	76.9 (0.3)	80.1 (0.5)	73.00
MVP-C	1	69.7 (0.9)	74.9 (0.5)	64.1 (0.5)	61.0 (1.4)	78.3 (2.7)	75.7 (1.5)	74.7 (0.8)	81.3 (0.7)	72.46
	5	72.4 (1.6)	74.4 (0.2)	63.1 (0.4)	63.9 (1.2)	77.5 (4.2)	75.0 (1.0)	77.0 (1.2)	81.2 (0.9)	73.07
	10	69.5 (1.5)	74.5 (0.5)	63.9 (0.9)	60.9 (0.4)	81.1 (1.8)	76.8 (1.5)	76.0 (0.8)	82.0 (1.0)	73.09
	20	72.1 (0.4)	73.4 (0.7)	63.9 (0.3)	63.0 (0.7)	78.8 (2.4)	74.1 (1.0)	74.8 (0.9)	84.1 (0.6)	73.02

G.3 ABLATION STUDY: EFFECT OF EACH LOSS COMPONENT

Table 11: Molecular graph property prediction, we set $C=5$ and $M=0.15$ for GraphMVP methods.

	BBBP	Tox21	ToxCast	Sider	ClinTox	MUV	HIV	Bace	Avg
# Molecules	2,039	7,831	8,575	1,427	1,478	93,087	41,127	1,513	-
# Tasks	1	12	617	27	2	17	1	1	-
-	65.4(2.4)	74.9(0.8)	61.6(1.2)	58.0(2.4)	58.8(5.5)	71.0(2.5)	75.3(0.5)	72.6(4.9)	67.21
InfoNCE only	68.9(1.2)	74.2(0.3)	62.8(0.2)	59.7(0.7)	57.8(11.5)	73.6(1.8)	76.1(0.6)	77.6(0.3)	68.85
EBM-NCE only	68.0(0.3)	74.3(0.4)	62.6(0.3)	61.3(0.4)	66.0(6.0)	73.1(1.6)	76.4(1.0)	79.6(1.7)	70.15
VAE only	67.6(1.8)	73.2(0.5)	61.9(0.4)	60.5(0.2)	59.7(1.6)	78.6(0.7)	77.4(0.6)	75.4(2.1)	69.29
AE only	70.5(0.4)	75.0(0.4)	62.4(0.4)	61.0(1.4)	53.8(1.0)	74.1(2.9)	76.3(0.5)	77.9(0.9)	68.89
InfoNCE + VAE	69.6(1.1)	75.4(0.6)	63.2(0.3)	59.9(0.4)	69.3(14.0)	76.5(1.3)	76.3(0.2)	75.2(2.7)	70.67
EBM-NCE + VAE	68.5(0.2)	74.5(0.4)	62.7(0.1)	62.3(1.6)	79.0(2.5)	75.0(1.4)	74.8(1.4)	76.8(1.1)	71.69
InfoNCE + AE	65.1(3.1)	75.4(0.7)	62.5(0.5)	59.2(0.6)	77.2(1.8)	72.4(1.4)	75.8(0.6)	77.1(0.8)	70.60
EBM-NCE + AE	69.4(1.0)	75.2(0.1)	62.4(0.4)	61.5(0.9)	71.1(6.0)	73.3(0.3)	75.2(0.6)	79.3(1.1)	70.94

G.4 BROADER RANGE OF DOWNSTREAM TASKS: MOLECULAR PROPERTY PREDICTION

Table 12: Results for four molecular property prediction tasks (regression). For each downstream task, we report the mean (and standard variance) RMSE of 3 seeds with scaffold splitting. For GraphMVP, we set $M = 0.15$ and $C = 5$. The best performance for each task is marked in **bold**.

	ESOL	Lipo	Malaria	CEP	Avg
-	1.178 (0.044)	0.744 (0.007)	1.127 (0.003)	1.254 (0.030)	1.07559
AM	1.112 (0.048)	0.730 (0.004)	1.119 (0.014)	1.256 (0.000)	1.05419
CP	1.196 (0.037)	0.702 (0.020)	1.101 (0.015)	1.243 (0.025)	1.06059
JOAO	1.120 (0.019)	0.708 (0.007)	1.145 (0.010)	1.293 (0.003)	1.06631
GraphMVP	1.091 (0.021)	0.718 (0.016)	1.114 (0.013)	1.236 (0.023)	1.03968
GraphMVP-G	1.064 (0.045)	0.691 (0.013)	1.106 (0.013)	1.228 (0.001)	1.02214
GraphMVP-C	1.029 (0.033)	0.681 (0.010)	1.097 (0.017)	1.244 (0.009)	1.01283

G.5 BROADER RANGE OF DOWNSTREAM TASKS: DRUG-TARGET AFFINITY PREDICTION

Table 13: Results for two drug-target affinity prediction tasks (regression). For each downstream task, we report the mean (and standard variance) MSE of 3 seeds with random splitting. For GraphMVP, we set $M = 0.15$ and $C = 5$. The best performance for each task is marked in **bold**.

	Davis	KIBA	Avg
-	0.286 (0.006)	0.206 (0.004)	0.24585
AM	0.291 (0.007)	0.203 (0.003)	0.24730
CP	0.279 (0.002)	0.198 (0.004)	0.23823
JOAO	0.281 (0.004)	0.196 (0.005)	0.23871
GraphMVP	0.280 (0.005)	0.178 (0.005)	0.22860
GraphMVP-G	0.274 (0.002)	0.175 (0.001)	0.22476
GraphMVP-C	0.276 (0.004)	0.168 (0.001)	0.22231

G.6 CASE STUDIES

Shape Analysis (3D Diameter Prediction). Diameter is an important measure in molecule [60, 62], and genome [22] modelling. Usually, the longer the 2D diameter (longest adjacency path) is, the larger the 3D diameter (largest atomic pairwise l2 distance). However, this is not always true. Therefore, we are particularly interested in using the 2D graph to predict the 3D diameter when the 2D and 3D molecular landscapes are with large differences (as in Figure 2 and Figure 8). We formulate it as a n -class recognition problem, where n is the number of class after removing the consecutive intervals. We provide numerical results in Table 14 and more visualisation examples in Figure 9.

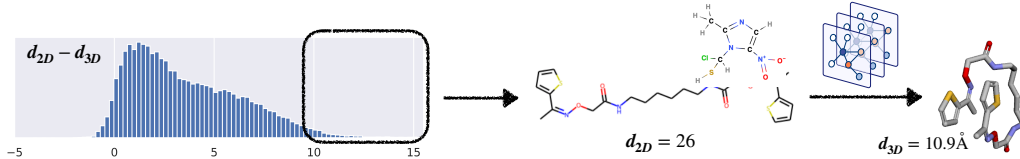


Figure 8: Molecules selection, we select the molecules that lies in the black dash box.

Long-Range Donor-Acceptor Detection. Donor-Acceptor structures such as hydrogen bonds have key impacts on the molecular geometrical structures (collinear and coplanarity), and physical properties (melting point, water affinity, viscosity etc.). Usually, atom pairs such as “O...H” that are closed in the Euclidean space are considered as the donor-acceptor structures [46]. On this basis, we are particularly interested in using the 2D graph to recognize (i.e., binary classification) donor-acceptor

Table 14: Accuracy on Recognizing Molecular Spatial Diameters

Random	AttrMask	ContextPred	GPT-GNN	GraphCL	JOAOv2	MVP	MVP-G	MVP-C
38.9 (0.8)	37.6 (0.6)	41.2 (0.7)	39.2 (1.1)	38.7 (2.0)	41.3 (1.2)	42.3 (1.9)	41.9 (0.7)	42.3 (1.3)

structures which have larger ranges in the 2D adjacency (as shown in Figure 2). Similarly, we select the molecules whose donor-acceptor are close in 3D Euclidean distance but far in the 2D adjacency. We provide numerical results in Table 15. Both tables show that MVP is the MVP :)

Table 15: Accuracy on Recognizing Long-Range Donor-Acceptor Structures

Random	AttrMask	ContextPred	GPT-GNN	GraphCL	JOAOv2	MVP	MVP-G	MVP-C
77.9 (1.1)	78.6 (0.3)	80.0 (0.5)	77.5 (0.9)	79.9 (0.7)	79.2 (1.0)	80.0 (0.4)	81.5 (0.4)	80.7 (0.2)

Chirality. We have also explored other tasks such as predicting the molecular chirality, it is a challenging setting if only 2D molecular graphs are provided [72]. We found that GraphMVP brings negligible improvements due to the model capacity of SchNet. We save this in the ongoing work.

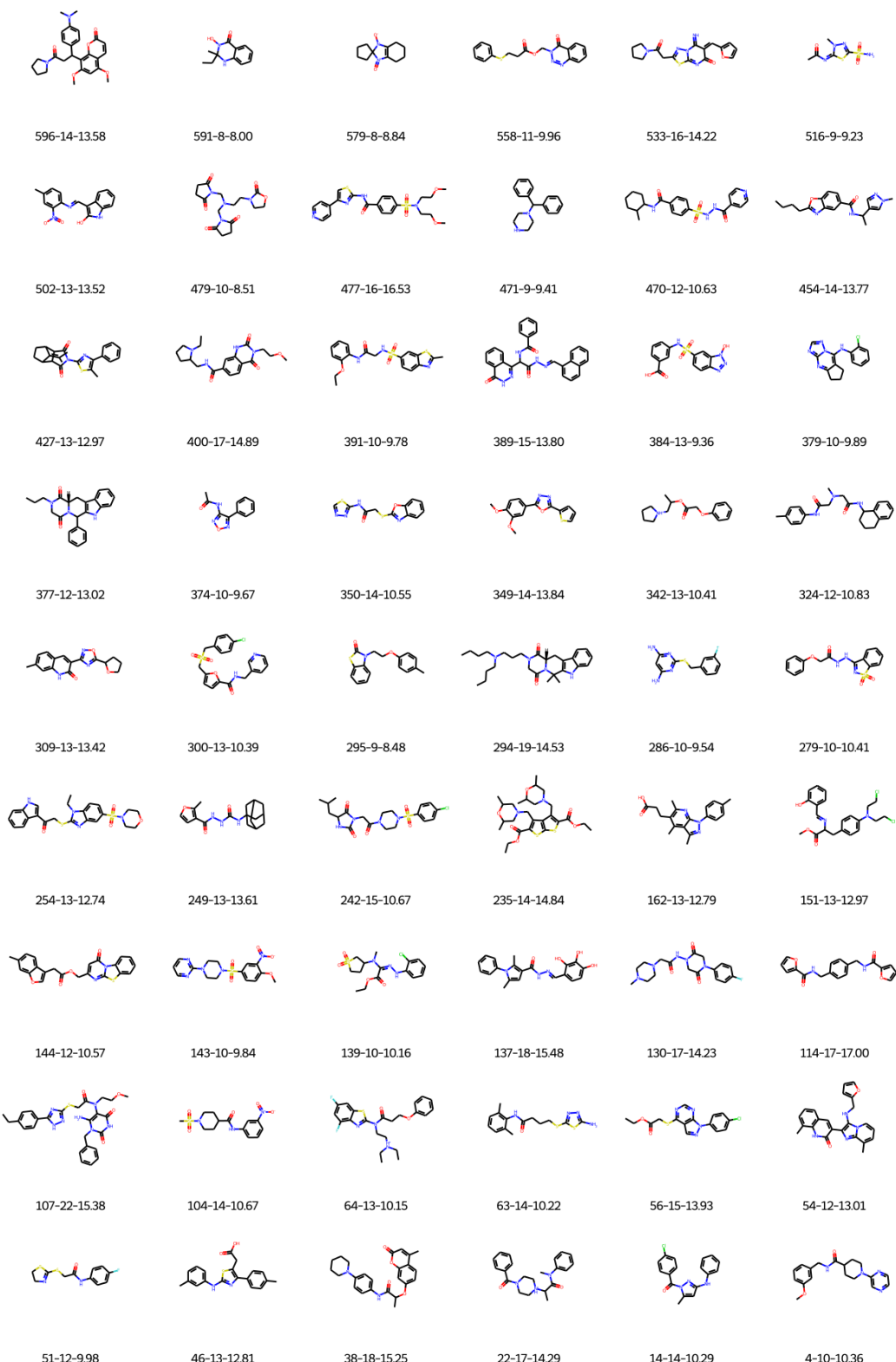


Figure 9: Molecule examples where GraphMVP successfully recognizes the 3D diameters while random initialisation fails, legends are in a format of “molecule id”-“2d diameter”-“3d diameter”.